JOURNAL OF PETROLOGY | VOLUME 40 | NUMBER 7 | PAGES 1065–1087 | 1999

Ultra-high Temperature Metamorphism of Metapelitic Granulites from Kondapalle, Eastern Ghats Belt: Implications for the Indo-Antarctic Correlation

P. SENGUPTA[1], J. SEN[1,3], S. DASGUPTA[1], M. RAITH[2]*, U. K. BHUI[1] AND J. EHL[2]

[1]DEPARTMENT OF GEOLOGICAL SCIENCES, JADAVPUR UNIVERSITY, CALCUTTA 700032, INDIA

[2]MINERALOGISCH–PETROLOGISCHES INSTITUT, UNIVERSITÄT BONN, POPPELSDORFER SCHLOSS, 53115 BONN, GERMANY

[3]ATOMIC MINERAL DIVISION, GOVERNMENT OF INDIA, LALCHAND BASTI, SHILLONG 793011, INDIA

RECEIVED FEBRUARY 1, 1998; REVISED TYPESCRIPT ACCEPTED JANUARY 8, 1999

A suite of quartz- and corundum-bearing metapelitic granulites, intruded by layered gabbronorite–pyroxenite–anorthosite at Kondapalle, Eastern Ghats Belt, preserves a multitude of reaction textures involving oxide and silicate minerals that attest to several prograde and retrograde reactions. In the quartz-bearing associations, the reactions are: (a) biotite + sillimanite + quartz → garnet + liquid; (b) garnet + sillimanite → spinel (+ magnetite) + quartz; (c) Fe_2TiO_4 + O_2 → ferrian ilmenite + magnetite; (d) reversal of reaction (b); (e) Fe_2O_3-rich ilmenite + plagioclase + quartz → Fe_2O_3-poor ilmenite + garnet + O_2. Reactions in the corundum-bearing associations are: (f) spinel + biotite + sillimanite → garnet + liquid; (g) biotite + sillimanite → garnet + Ti-rich spinel + corundum + liquid; (h) biotite + sillimanite → garnet + corundum + liquid; (i) Fe_2TiO_4 + $FeAl_2O_4$ + O_2 → ferrian ilmenite + Fe_3O_4 + Al_2O_3 (in ilmenite); (j) garnet + corundum → spinel + sillimanite. To examine the paragenetic evolution of the metapelitic granulites, a petrogenetic grid for the KFMASH system at high temperatures and pressures, involving quartz and corundum, was constructed. The sequence of inferred reactions documents an anticlockwise heating–cooling path. Re-integrated compositions of spinel (with >10 mol % Fe_2TiO_4) and feldspars indicate ultra-high temperature (UHT) of metamorphism (>1000°C), comparable with the liquidus temperature of the enclosing magmatic rocks. Crystallization pressures inferred for the magmatic rocks and the pressure constraints imposed by the petrogenetic grid on the metapelite assemblages indicate that the emplacement of the igneous suite and the accompanying UHT metamorphism occurred in the lower crust (>8 kbar). Reported U–Pb cooling ages of monazite and allanite from a late pegmatite suggest the UHT metamorphism to be older than 1600 Ma. The deduced P–T *history and the absence of Grenvillian high-grade metamorphism in the study area provide important constraints on the configuration of East Gondwana, in particular on the continuation of the Napier–Rayner terrane boundary into the Eastern Ghats Belt.*

KEY WORDS: *metapelitic granulites; UHT metamorphism; Eastern Ghats Belt, India; Indo-Antarctic terrane assembly*

INTRODUCTION

Detail petrological investigations over the last decade have identified a small number of regional granulite facies terranes that underwent UHT metamorphism (ultra-high temperature >950°C) similar to pelitic xenoliths in basaltic magma [reviewed by Harley (1989, 1992), Hensen & Harley (1990) and Dasgupta & Sengupta (1995); references therein]. Thermal modelling of these terranes has indicated that advective heat transfer is

*Corresponding author. Telephone: +49-228-732933. Fax: +49-228-732763. e-mail: m.raith@uni-bonn.de

necessary to achieve such extreme temperatures of metamorphism, and intrusion of hot basic melts is commonly invoked as the cause (Wickham & Oxburgh, 1985; Harley, 1989, 1992; references therein). Under- or interplating of voluminous basic magma accompanied by granulite facies metamorphism and consequent granite production are considered to be an important process for the formation of the lower crust and for crustal differentiation (Ellis & Green, 1985; Bohlen, 1987; Clemens & Vielzeuf, 1987; Frost & Frost, 1987; Harley, 1989, 1992, and the references cited therein). However, intrusion of voluminous high-temperature basic magmas and accompanying UHT metamorphism in the lower crust are documented from only a few regional granulite terranes [reviewed by Harley (1992)]. Interpretation of coronitic and symplectitic reaction textures in Mg–Al granulites together with geothermobarometry in the enclosing basic and felsic granulites have demonstrated that these UHT granulites dominantly show near-isobaric cooling subsequent to peak temperatures (Harley, 1989, 1992; Dasgupta & Sengupta, 1995). Unfortunately, apart from a few exceptions (e.g. Hensen & Motoyoshi, 1988; Sengupta *et al.*, 1990; Goscombe, 1992; Dasgupta *et al.*, 1995; Mukhopadhyay & Bhattacharya, 1997; Raith *et al.*, 1997), the UHT metamorphism has obliterated the signatures of the prograde reaction history. As a consequence, the geodynamic milieu of most of the UHT granulites remains obscure (Harley, 1989, 1992).

The Eastern Ghats orogenic belt along the east coast of India (Fig. 1) preserves vestiges of UHT metamorphism with a characteristic retrograde near-isobaric cooling P–T path [reviewed by Dasgupta & Sengupta (1995)]. Reassembly of East Gondwana has juxtaposed the Eastern Ghats Belt against parts of East Antarctica [between 40 and 70°E longitude; see Federov *et al.* (1982), Grew *et al.* (1988), Unrug (1995) and Yoshida (1995)]. Hence, identification and characterization of metamorphic events in the Eastern Ghats Belt and their comparison with the evolutionary history of the East Antarctic granulites are crucial, not only to understanding the spatial and temporal variation of Precambrian orogenic processes, but also to provide important and independent constraints on the configuration of East Gondwana before ~500 Ma [see Federov *et al.* (1982), Grew *et al.* (1988), Unrug (1995) and Yoshida (1995) among others].

Extensive geological and geochronological investigations on the rocks of East Antarctica have identified three major metamorphic events broadly at late Archaean, Grenvillian and Pan-African times [reviewed by Harley & Hensen (1990) and Harley & Fitzsimons (1995)]. One of the outstanding features of the Archaean Napier complex is UHT metamorphism ($T > 1000$°C) followed by near-isobaric cooling at different crustal depths. This strongly contrasts with the bordering Rayner complex of

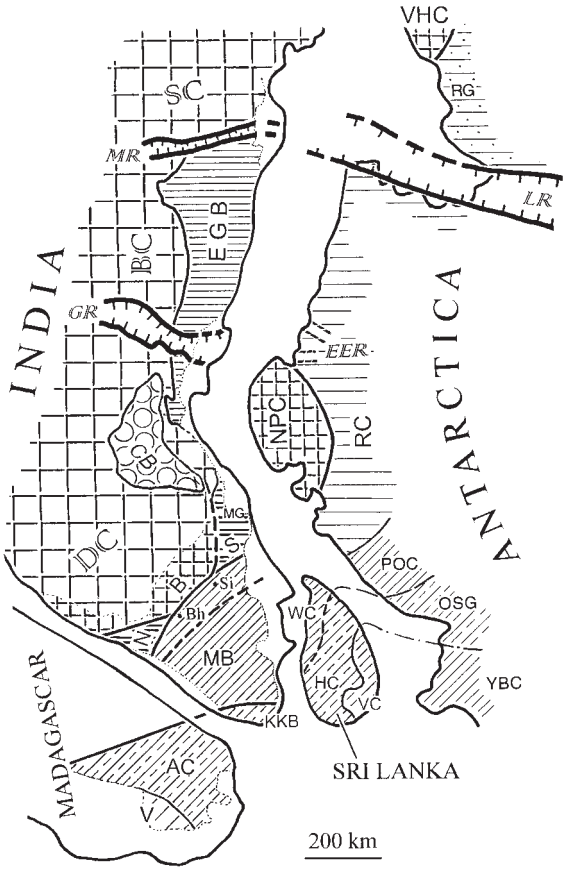

Fig. 1. Assembly of East Gondwana showing the position of the Eastern Ghats Belt (compiled by M. Raith). India: DC, BC and SC, Middle to Late Archaean Dharwar, Bhandara and Singhbhum cratons, respectively; N, B and S, Late Archaean to Early Proterozoic granulites of the Nilgiri, Biligirirangan and Shevaroy hills, respectively; Bh and Si, Bhavani and Sittampundi layered basic intrusions; MB, granulite terrane of Madurai [Early(?) or Middle(?) Proterozoic to Pan-African]; KKB, Kerala khondalite belt (Pan-African); EGB, Eastern Ghats Belt; CB, Middle Proterozoic Cuddapah sedimentary sequences (metamorphosed only on the eastern margin); MR and GR, Mahanadi and Godavari rifts. Southern Madagascar: AC and V, granulite facies rocks (Pan-African) of the Androyen complex and Vohibory terrane. Sri Lanka: VC, HC and WC, Neo-Proterozoic Vijayan (amphibolite facies), Highland (granulite facies) and Wanni (both amphibolite and granulite facies) complexes. East Antarctica: NPC and VHC, Archaean Napier and Vestfold Hill complexes (both granulite facies), RG, RC, POC, OSG, YBC, Neo-Proterozoic (with Pan-African overprint) Rauer group, Rayner complex, Prince Olav complex, Ongul–Skallen group and Yamato–Belgica complex. LR and EER, Lambert and East Enderby rifts. The bold lines are crustal-scale shear zones in East Gondwana.

Grenvillian age (~1000 Ma). The latter is characterized by distinctly lower peak temperature (750–850°C) followed by a stage of near-isothermal decompression [reviewed by Harley & Hensen (1990)]. However, vestiges of UHT metamorphism and the subsequent near-isobaric cooling, believed to be of Archaean age, are also documented in a few low strain zones within the Rayner complex which has produced complex P–T loops [see

Harley & Hensen (1990)]. The boundary between the Napier and Rayner complexes (hereafter, N–R boundary) marks the border of the ~1000 Ma orogeny in East Antarctica and, hence, location of this boundary in the Eastern Ghats Belt has implications for the global Southwest US–East Antarctic (SWEAT) connection in general, and the relative position of India and Antarctica in the Precambrian time, in particular [see Unrug (1995)]. However, in comparison with East Antarctica, geological and geochronological information from the Eastern Ghats Belt is meagre and is essentially restricted to a few scattered areas north of the Godavari Rift (the segments north and south of the Godavari rift will be hereafter referred to as the northern and southern sectors, respectively; Fig. 1). It is evident from the palaeomagnetic fitting of these two continents that the southern sector of the Eastern Ghats Belt is juxtaposed predominantly against the Napier complex of East Antarctica (Fig. 1). Therefore, limited petrological and geochronological information from this sector [see Dasgupta *et al.* (1997)] is a major handicap in the comparison of the geological history of these two erstwhile neighbouring continents and hence, delineation of the N–R boundary in this belt.

Against this background, we present textural features and compositional characteristics of oxide and silicate minerals from a suite of metapelitic granulites (khondalites) that are intercalated with a volumetrically dominant gabbronorite–anorthosite suite of rocks from the layered magmatic complex of Kondapalle (Figs 1 and 2). We also present the salient petrological characteristics of the enclosing layered mafic rock suite for a better understanding of the physico-chemical milieu of the khondalites. Incidentally, the Kondapalle layered complex is the only example of its kind in the entire Eastern Ghats Belt [discussed by Leelanandam (1990)]. Although the exact timing of granulite facies metamorphism in the southern sector is not yet known, recent U–Pb cooling dates of monazite and allanite from a late pegmatite suggest that the last high-grade metamorphism in this area is older than 1600 Ma (Mezger *et al.*, 1996; Mezger & Cosca, 1999). Combining the petrological data presented here with information on other well-studied areas and the available geochronological data, continuation of the N–R boundary in the Eastern Ghats Belt has been evaluated.

BACKGROUND GEOLOGY

The study area of Kondapalle is situated in the southern segment of the Eastern Ghats Belt close to the Godavari rift (Fig. 1). Because of the occurrence of a layered magmatic complex and associated chromite ores, the area has been investigated by a number of workers for more than four decades [reviewed by Leelanandam (1990, 1997)]. Nanda & Natarajan (1980) first undertook large-scale mapping of the area and presented a good general description of the different lithologies, their mutual relations and deformational history. Subsequent detailed mapping and petrological investigation of the different rock types by the authors of the present paper have considerably modified the work of Nanda & Natarajan (1980). The distribution of the different lithologies and the generalized geological history are presented in Fig. 2 and Table 1.

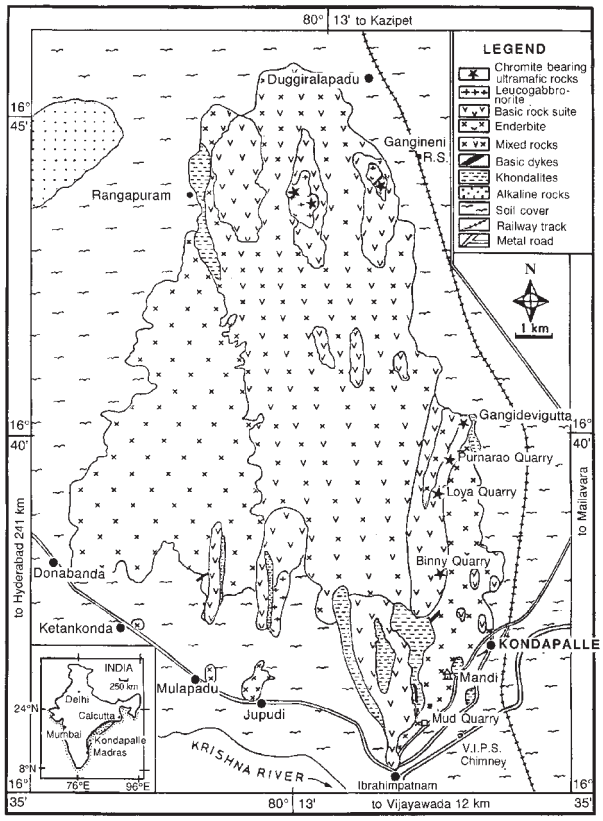

Fig. 2. Geological map of the Kondapalle area.

The study area is dominated by several magmatic rocks including the gabbronorite–pyroxenite–anorthosite layered complex and later enderbite to charnoenderbite intrusives. The mafic–ultramafic layered complex predominantly consists of gabbronorite which, in places, grades into leucogabbronorite to anorthosite. The last two rocks show magmatic layering defined by alternate pyroxene- and plagioclase-rich bands. Clinopyroxenite (locally with orthopyroxene and plagioclase) and chromite-bearing enstatitite are the dominant ultramafic rocks in the study area. The former rock occurs as thin to thick layers or pods of various dimensions in all these mafic members, whereas large pods of the latter rock (often several metres in length) are found only in the leucogabbronorite and anorthosite. Layering (centimetres

Table 1: Generalized geological history of the Kondapalle area

young	Development of N–S ductile shear zones, fluid fluxing and formation of retrograde hydrous and carbonatic phases in all litho-units. Ar–Ar cooling age of hornblende ~1100 Ma
	Emplacement of allanite-bearing granitic pegmatite. U–Pb cooling ages of allanite (~1600 Ma) and monazite (1672 Ma)
	Emplacement of dolerite dyke
	F_2–F_4 folding, emplacement of noritic dyke along F_3
	Emplacement of pegmatoidal enderbite
	F_1 recumbent folding, emplacement of enderbite–charnoenderbite along the axial plane (S_2)
	Emplacement of basic magma, fractionation (ultramafic–basic-anorthosite) at 35–40 km depth, UHT metamorphism of the pelitic rocks, partial melting and segregation of leucosomes and melanosomes (S_1)
old	Deposition of supracrustal rocks (mainly pelites)

up to 2 m) of chromite and enstatite is a common feature of this rock. The enderbite–charnoenderbite (garnet + antiperthitic plagioclase + quartz + orthopyroxene ± perthite) occurs in two modes. One is massive to gneissic and the other is pegmatoidal. Lit-par-lit injection of the first type into the mafic–ultramafic rocks has developed conspicuous layering. This type of enderbite–charnoenderbite also contains xenoliths or rafts of rocks of the layered complex and the intercalated khondalites. The gneissic banding of the enderbite–charnoenderbite often warps around these xenoliths or rafts. The most abundant of the xenoliths are clinopyroxene- and hercynite-bearing orthopyroxenite. Extensive metasomatic veining of quartz with or without plagioclase occurs in the mafic–ultramafic rocks and/or the khondalite at the contact of enderbite–charnoenderbite. The field relations among the mafic–ultramafic and the enderbitic rocks are strikingly similar to those described from the Madras area (Subramaniam, 1959). The pegmatoidal enderbite occurs as ramifying veins cutting across the gneissic banding of the enderbitic rocks.

Khondalites, which are the subject of the present study, occupy only a minor proportion of the exposed area (<10 vol. %, Fig. 2). These rocks show melanocratic and leucocratic layering in the centimetre to metre scale.

In the north-western part of the study area, a suite of alkaline rocks (ranging from quartz syenite to alkali granite) is recorded for the first time from this area. The other rock types include basic dykes and several generations of pegmatite.

The rocks of the study area were affected by polyphase deformation. The earliest recognizable structure is shallowly dipping (10–20°) recumbent folds (F_1) defined by the migmatitic and the magmatic layering in khondalite and mafic–ultramafic rocks, respectively. The most pervasive planar structure is a shallowly dipping foliation (S_1) axial planar to F_1. The lit-par-lit injection of the enderbite–charnoenderbite also occurred along this planar structure. The S_1 planar structure has subsequently been modified by at least three sets of folds (F_2–F_4). Interference of these folds has resulted in a complex outcrop pattern in the layered rocks. Subsequently, allanite–monazite-bearing pink pegmatite was intruded. Finally, a set of roughly N–S trending subparallel shear zones (dip >70°E to almost subvertical) have cut across all the rock types, including the pegmatite. The host rocks in the shear zones show extensive recrystallization and development of amphibole. Allanite and monazite from the pegmatite have yielded U–Pb cooling ages of 1672 ± 4 Ma (monazite) and ~1600 Ma (allanite), and the ^{40}Ar–^{39}Ar age of a retrograde hornblende from the shear zone is ~1100 Ma (Mezger *et al.*, 1996; Mezger & Cosca, 1999). The field features (described above) and these mineral age data, thus, collectively indicate that the high-grade metamorphism of khondalites is older than 1640 Ma. This is the first unequivocal documentation of pre-Grenvillian granulite facies metamorphism in the Eastern Ghats Belt. The ~1100 Ma ^{40}Ar–^{39}Ar amphibole age documents a localized Grenvillian thermal overprint (up to amphibolite facies). The U–Pb cooling ages of allanite and monazite further suggest that the Grenvillian granulite facies metamorphism, which is pervasive in the northern sector (see Grew & Manton, 1986; Aftalion *et al.*, 1988; Paul *et al.*, 1990; Mezger *et al.*, 1996), is absent in the study area. The implication of this will be discussed later.

METAMORPHIC EVOLUTION OF KHONDALITES

Reaction textures

In this section, the mutual relations between the different phases and their compositions are described (see Tables 2–6). In view of their diversity and complexity, the oxide intergrowths are discussed separately.

Table 2: Representative mineral compositions from the members of the layered magmatic complex

Rock:	Spl-orthopyroxenite					Spl-orthopyroxenite					clinopyroxenite			chr-enstatitite		Type-I mafic granulite			leucogabbronorite		
Sample:	K6B					K264C					K264			K65		K36	K35		K39		
Mineral:	ol	spl	opx	amp	grt	spl	opx	cpx	plag	gt	cpx	plag	gt	chr-spl	opx	cpx*	cpx	plag	cpx	opx	plag
SiO_2	37·68	0·01	51·16	43·35	39·11	0·04	54·00	49·27	43·76	39·13	51·42	44·86	38·44		56·35	50·05	50·42	49·09	52·46	51·15	46·66
TiO_2	0·01	0·06	0·25	0·65		0·04	0·11	0·81		0·28	0·02		0·01	0·09	0·04	0·13	0·48	0·02	0·01	0·04	
Al_2O_3	0·01	56·98	3·33	13·07	21·76	59·07	1·18	5·1	36·17	21·56	0·58	34·67	21·37	18·11	2·02	1·89	3·15	32·51	1·61	2·10	34·12
Cr_2O_3		0·06	0·02			0·11	0·39	0·04	0·01	0·03			0·04	48·07	0·37	0·09	0·28				0·01
FeO	22·82	29·76	18·99	9·27	20·60	25·3	14·96	5·36	0·19	17·10	12·02	0·10	23·89	22·88	5·24	11·43	7·73	0·37	8·48	24·69	0·02
MnO	0·71	0·31	0·66	0·13	2·70	0·42	0·24	0·42	0·02	3·19	0·61	0·01	3·26	0·21	0·11	0·32	0·12	0·05	0·18	0·74	0·01
MgO	38·52	11·12	24·44	15·82	7·00	13·55	29·42	15·19	0·01	9·05	11·98	0·02	2·88	9·58	35·75	14·52	14·33	0·01	14·50	21·49	
CaO			0·27	12·21	9·55	0·03	0·54	23·46	20·00	9·01	22·56	17·32	10·07	0·01	0·19	18·94	21·88	15·91	22·54	0·03	17·43
Na_2O				2·12		0·02	0·01	0·19	0·17		0·30	1·02		0·02		0·59	0·65	2·62	0·43	0·02	1·56
K_2O			0·01	0·76	0·03	0·01						0·04						0·10	0·02		0·01
Total	99·77	98·30	99·13	97·37	100·85	98·59	100·85	99·84	100·35	99·35	99·49	98·05	99·96		100·07	97·95	99·04	100·7	100·22	100·53	100·10
Oxygen	4·00	4·00	6·00	22·00	12·00	4·00	6·00	6·00	8·00	12·00	6·00	8·00	12·00	4·00	6·00	6·00	6·00	8·00	6·00	6·00	8·00
Si	0·99		1·99	6·32	2·99		1·95	1·83	2·02	2·99	1·97	2·10	3·02		1·93	1·92	1·90	2·23	1·95	1·92	2·14
Ti			0·01	0·07				0·02									0·01				
Al		1·85	0·14	1·66	1·96	1·88	0·05	0·22	1·97	1·95	0·03	1·91	1·98	0·69	0·08	0·09	0·14	1·74	0·07	0·09	1·85
Fe^{3+}		0·15				0·11	0·04	0·09	0·01		0·05			0·08	0·05	0·10	0·08	0·01	0·05	0·06	0·01
Cr							0·01							1·23	0·01		0·01				
Fe^{2+}	0·50	0·39	0·59	1·13	1·32	0·45	0·40	0·08		1·09	0·33		1·57	0·53	0·10	0·26	0·16		0·21	0·71	
Mn	0·02	0·01	0·02	0·01	0·17	0·01	0·01	0·01		0·21	0·02		0·21			0·01				0·02	
Mg	1·56	0·61	1·35	3·43	0·80	0·54	1·53	0·84		1·03	0·68		0·34	0·46	1·83	0·83	0·80		0·80	1·20	
Ca			0·01	1·79	0·78		0·02	0·93	0·99	0·74	0·92	0·87	0·85			0·78	0·89	0·78	0·90	0·01	0·86
Na				0·60				0·01	0·01		0·02	0·09				0·04	0·04	0·23	0·03		0·14
K				0·14														0·01			
X_{Mg}	0·75		0·70	0·75	0·26	0·54	0·79	0·91		0·48	0·67		0·18	0·46	0·95	0·76	0·45		0·79	0·63	

X_{Mg}, $Mg/(Mg + Fe^{2+})$.
*Reintegrated composition.

Ferromagnesian layers in the migmatitic khondalite show mineralogical variations even within a few centimetres. Two associations are identified on the basis of characteristic minerals. Association I can be distinguished from the other by the presence of quartz and absence of porphyroblastic corundum. The mineralogy of the two associations is given below:

Association I: garnet–spinel (with magnetite)–sillimanite–quartz–(Fe–Ti) oxides–perthite–plagioclase–biotite–sulphide minerals;

Association II: garnet–spinel (with magnetite)–corundum–sillimanite–(Fe–Ti) oxide–perthite–plagioclase–biotite–sulphide minerals.

In most places the mutual relations among the phases are partially to completely obliterated as a result of superimposed deformation. Replacement of the anhydrous phases, such as garnet, spinel and perthite, by biotite + quartz, biotite + quartz + sillimanite, or biotite + sillimanite is frequently observed. This retrograde biotite defines a schistosity which often swerves around and replaces the porphyroblastic phases. This schistosity is parallel to the regional pervasive foliation S_2. However, a few zones of relatively low strain preserve pre-deformational reaction textures that are described below.

Two generations of garnet, one porphyroblastic [hereafter garnet (1)] and the other coronal [hereafter garnet (2)] occur in both the associations. In association I, garnet (1) includes one or more of the phases biotite, sillimanite, quartz and plagioclase. Garnet (1) is frequently embayed by lobate spinel. These spinel grains are rimmed against quartz by garnet (2) and sillimanite of various thickness (Fig. 3a). Srogi *et al.* (1993) interpreted a similar texture as two-stage garnet growth, i.e. before and after the formation of spinel. In association II, biotite and sillimanite are the dominant inclusions in garnet (1), quartz being present in only a few garnet (1) grains. In places, small granular inclusions of spinel with one or both of the phases biotite and sillimanite occur in the core of garnet (1) (Fig. 4a). Commonly, garnet (1) forms clusters with porphyroblastic corundum and spinel [hereafter, corundum (1) and spinel (1)] (Fig. 4b). Garnet (1) is often replaced by coarse intergrowths of spinel and sillimanite at the contact of corundum (1) (Fig. 4a).

Spinel is hercynitic and has three modes of occurrence. Small granular spinel occurs as inclusions along with biotite with or without sillimanite in the core of garnet (1) in association II (Fig. 4a). This spinel is likely to have formed before garnet (1). The most abundant variety is porphyroblastic [i.e. spinel (1)] that embays garnet (1) in both the associations. This variety frequently forms coarse aggregates with ilmenite and invariably shows crystallographically controlled intergrowths with magnetite in both the associations. Details of the oxide intergrowths will be discussed separately. In association I, spinel (1) is separated from quartz by either garnet (2) or a compound corona of sillimanite and garnet (Fig. 3a). In association II, spinel (1) often forms coarse intergrowths with sillimanite laths that replace garnet (1) (Fig. 4a).

Coarse ilmenite in association I is rimmed by garnet (2) against plagioclase and quartz. Garnet (2) is found to be intergrown with granular ilmenite (Fig. 3b).

Two generations of biotite are identified. Primary biotite that existed before garnet (1) mostly occurs as inclusions in the latter. In none of the associations does primary biotite coexist with sillimanite or quartz in the matrix. Secondary biotite is profusely developed in zones of intense deformation and defines the S_2 fabric. This biotite replaces garnet (1) and other anhydrous phases along cracks and fractures. In places, delicate intergrowths of sillimanite and secondary biotite are observed.

Corundum occurs in a variety of forms. Porphyroblastic corundum [i.e. corundum (1)] coexists with garnet (1) and spinel (1) in association II. Corundum also forms complex intergrowths with spinel and ilmenite in this association.

K-feldspar in both the associations is perthitic with numerous blebs and/or lamellae of plagioclase. It is mostly concentrated in the leucocratic bands along with quartz and plagioclase. A few grains of plagioclase are antiperthitic.

Sillimanite exhibits several textural varieties. The earliest occurs as inclusions in garnet (1) in both the associations. In association I sillimanite rims spinel (1) against quartz (Fig. 3a). In association II, haphazardly oriented coarse blades of sillimanite are intergrown with spinel and replace garnet (1) (Fig. 4a).

Oxide minerals in the study rocks show spectacular intergrowths. Spinel (1) in both the associations forms dendritic intergrowths with magnetite of variable thickness and length (Fig. 4c). The coarsest magnetite lamellae are invariably deformed to various extents and have tensional cracks. In places laths of corundum and/or sillimanite are also present in spinel (1) (Fig. 4c). In places, granules of magnetite often occur along the spinel–corundum contacts (Fig. 4c). The volume proportion of magnetite in spinel (1) never exceeds 15%. Magnetite never forms free grains in the matrix. This feature, together with rimming of spinel (1) by coronitic garnet, suggests that magnetite exsolved after the formation of the coronal garnet (see Waters, 1991). Coarse ilmenite grains invariably show fine lamellae of Ti-haematite (Fig. 4d). This feature is common in many magmatic and high-grade metamorphic rocks and is formed as a result of unmixing from a homogeneous Fe_2O_3-rich ilmenite during cooling (Haggerty, 1976). Spinel (1) in both associations often forms coarse aggregates with

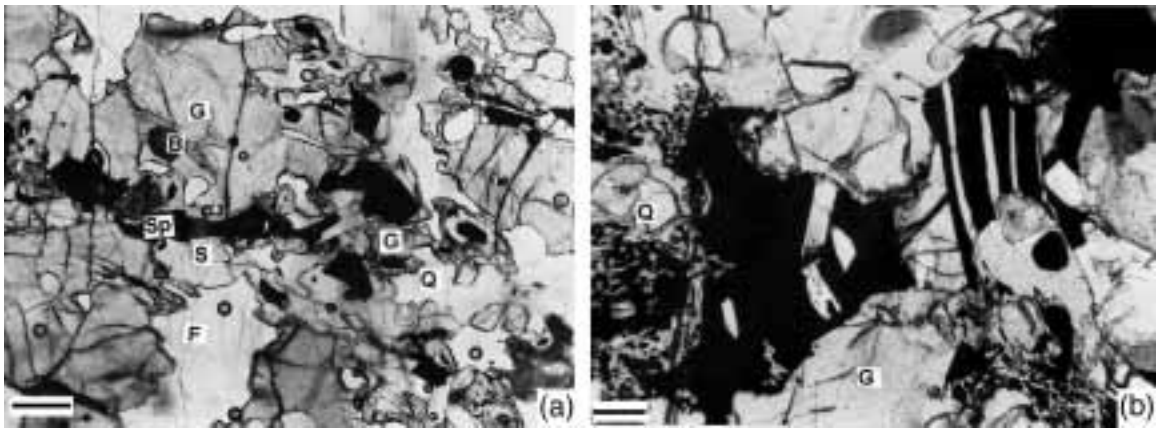

Fig. 3. Photomicrographs illustrating reaction textures in association I. (a) Garnet (1) (G) is embayed by spinel (Sp) which is in turn rimmed by garnet (2) and sillimanite (S) against quartz (Q). Coarse alkali feldpar (F) and biotite (B) inclusion in garnet (1) are also seen. Bar represents 200 μm. (b) Porphyroblastic ilmenite (black) is rimmed by an intergrowth of garnet (2) and granular ilmenite against quartz (Q). [Also note the lamellar intergrowth of corundum (C) and ilmenite (black).] Bar represents 200 μm.

ilmenite (Figs 3 and 4). The oxide–oxide contacts of the aggregates are straight. In most places, these aggregates preserve the shape of the original spinel grain, suggesting that they are the products of unmixing of a homogeneous spinel rich in TiO_2 (Haggerty, 1976; Waters, 1991). As the solubility of ilmenite in the spinel structure or vice versa is insignificant, the pristine spinel must have been rich in Fe_2TiO_4 (ulvöspinel). This component upon oxidation produced the present oxide aggregates [the granular exsolution of Buddington & Lindsley (1964); see Haggerty (1976) and Waters (1991)]. The volume proportion of ilmenite in most of these aggregates ranges from 20% to >35%, suggesting a significant proportion of Fe_2TiO_4 component in the original spinel (>19 mol %, Table 3). This is much higher than most of the other reported occurrences [see Waters (1991) and Fitzsimons (1996)]. Some composite oxide aggregates show spectacular intergrowths of corundum–spinel–ilmenite (Fig. 4e). In these aggregates corundum forms lamellar intergrowths with ilmenite which have sharp and straight boundaries with spinel. The spinel shows dendritic magnetite lamellae whereas ilmenite exsolves Ti-haematite lamellae. Mutual relations of the oxide phases in such composite grains also suggest the former existence of a homogeneous Fe–Ti–Mg–Al spinel. However, the corundum–ilmenite lamellar intergrowths also occur without spinel in places (Fig. 3b). Unlike other reported spinel-bearing occurrences (see Waters, 1991), the Fe–Ti–Al oxide aggregates are not rimmed by continuous garnet coronas and, in places, spinel and ilmenite are separated by garnet (2) and/or sillimanite (Fig. 4f).

Mineral chemistry

Chemical composition of the phases was determined with a CAMECA MICROBEAM electron microprobe at the University of Bonn. The instrument was operated with 15 kV accelerating voltage, 1–2 mm beam diameter and 15 nA current. However, for area scans the beam diameter was broadened up to 50 mm. At least four area scans were measured for each reintegration. Natural mineral standards were used and the raw electron probe microanalysis (EPMA) data were corrected by the PAP procedure (Pouchou & Pichoir, 1984).

Spinel is primarily an $MgAl_2O_4$–$FeAl_2O_4$ solid solution with X_{Mg} [$= Mg/(Mg + Fe^{2+})$] varying from 0·38 to 0·43 (Table 3). ZnO content in spinel is always low (<1 wt %) except in the small spinel granules in garnet (1), which contain higher amounts of ZnO (3·5 wt %, Table 3). The spot analyses of this mineral are always more magnesian than the coexisting garnet (Table 7). The presence of dendritic magnetite in spinel and the granular exsolution of ilmenite indicate that the pristine spinel was richer in Fe and Ti. The composition of the pristine spinel is not only crucial to understanding the peak thermal history of the host rock, but also has an important bearing on the topology of the system FeO–MgO–Al_2O_3–SiO_2 (FMAS) [see Waters (1991)]. Estimation of the pristine spinel composition in the studied rock is fraught with difficulties, such as: (1) the wide modal variation of ilmenite in the oxide aggregates; (2) the presence of variable contents of magnetite and Ti-haematite lamellae in spinel and ilmenite, respectively; (3) the absence of a continuous coronal phase, which makes it difficult to estimate the proportion of the different oxides in an aggregate; (4) the involvement of corundum lamellae in the intergrowth. The last problem has been circumvented by choosing aggregates devoid of corundum lamellae for integrated analyses. In view of point (3), we have chosen aggregates that contain a smaller proportion of ilmenite (20–25 vol. %) than the others. Bulk compositions of such aggregates are likely to provide

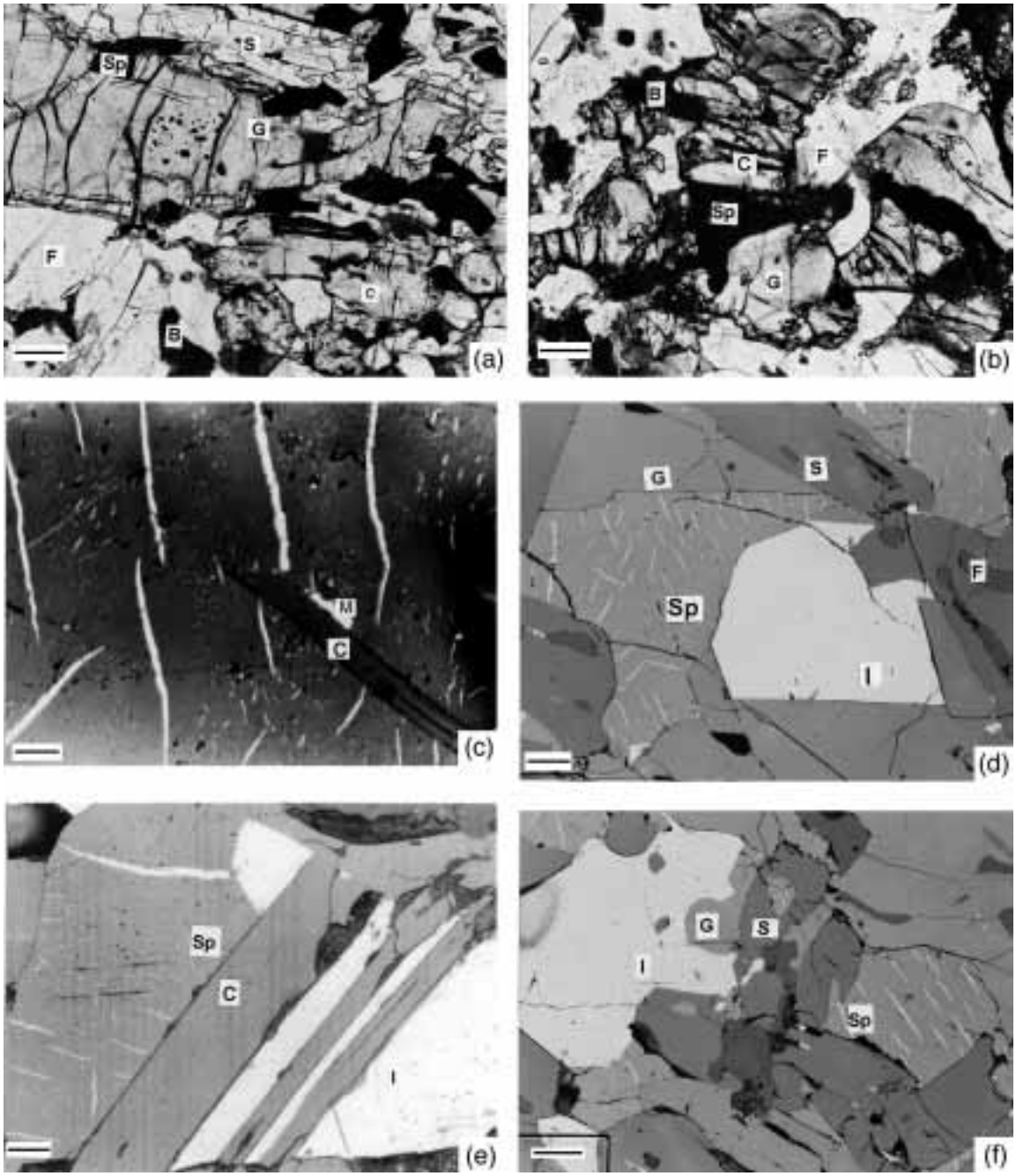

Fig. 4. Photomicrographs illustrating reaction textures in association II. (a) Garnet (1) (G) is replaced by a coarse intergrowth of sillimanite (S) and spinel (Sp) against corundum (1) (C). Note the inclusion of granular early spinel and biotite in garnet (1). F, alkali feldspar; B, retrograde biotite. Bar represents 200 μm. (b) Cluster of garnet (1), corundum (C) and spinel (Sp). F and B are retrograde alkali feldspar and biotite. Bar represents 200 μm. (C) Coarse spinel (grey base) with deformed dendritic magnetite lamellae (white). A slab of corundum (C) in spinel. [Note the localization of magnetite granules (M) along the contact of spinel and the corundum lath.] Bar represents 100 μm. (d) Coarse aggregate of spinel (Sp) and ilmenite (I). The dendritic lamellae of magnetite in spinel and fine Ti-haematite lamellae (bright) in ilmenite are also seen. [Note the sharp contact among the oxide grains.] Outline of the pristine spinel is still present (see text). Sillimanite (S) and garnet (G) are similar to those in (a). Bar represents 50 μm. (e) Composite aggregate of corundum (C), spinel (Sp) and ilmenite (I). Corundum forms lamellar intergrowth with ilmenite. Bar represents 50 μm. (f) Garnet (2) (G) and sillimanite (S) separating spinel (Sp) from ilmenite (I). Bar represents 50 μm.

a conservative estimate of Fe_2TiO_4 content in the pristine spinel. For reconstruction of the pristine spinel composition, the procedure mentioned by Waters (1991) was followed. The representative reintegrated compositions are presented in Table 3. The reintegrated compositions show significant ulvöspinel component (up to 17 mol %)

Table 3: Representative spinel compositions

Association:	I	I	I	I	II	II	II	II	I	I	II
Sample:	k671	k672	k673	k674	k676	k678	k680	k682	k671a	k671b	k676c
SiO_2	0·01			0·04	0·02			0·21	0·03		0·02
TiO_2			0·01	0·02		0·03		0·04	8·60	9·40	8·69
Al_2O_3	59·61	58·09	58·94	59·34	57·12	58·60	59·35	56·87	41·77	39·55	39·62
Cr_2O_3	0·34	0·36	0·27	0·03	0·52	0·26	0·46	1·15	0·04	0·25	0·30
FeO*	29·53	31·25	30·47	31·25	29·31	31·22	29·01	29·06	41·73	42·16	42·98
MnO	0·04		0·07	0·06	0·01	0·04	0·09		0·04	0·03	0·03
MgO	9·58	8·72	8·62	8·97	8·55	8·14	9·24	9·67	6·55	6·62	6·63
ZnO	0·40	0·26	0·27	0·23	3·49	0·29	0·37	0·39	0·16	0·26	
Total	99·51	98·31	98·65	99·94	99·43	98·58	98·52	97·39	98·92	98·27	99·02
Oxygen	4·00	4·00	4·00	4·00	4·00	4·00	4·00	4·00	4·00	4·00	4·00
Si											
Ti											
Al	1·94	1·92	1·93	1·93	1·89	1·93	1·94	1·89			
Fe^{3+}	0·06	0·07	0·07	0·07	0·06	0·06	0·06	0·11			
Cr	0·01	0·01	0·01		0·01	0·01	0·01	0·03			
Fe^{2+}	0·62	0·66	0·64	0·65	0·57	0·67	0·62	0·58			
Mn				0·01							
Mg	0·39	0·37	0·36	0·37	0·36	0·34	0·38	0·40			
Zn	0·01	0·05	0·01	0·03	0·07	0·01	0·01	0·01			
X_{Mg}	0·39	0·36	0·36	0·36	0·39	0·36	0·38	0·41	0·24	0·25	0·25
$X_{Fe^{3+}}$	0·03	0·03	0·04	0·03	0·03	0·03	0·03	0·05	0·09	0·10	0·12
Usp%									18·03	19·70	18·20

a, b and c are reintegrated pristine spinel compositions (see text).
Usp%, ulvöspinel mol %; X_{Mg}, Mg/(Mg + Fe^{2+}); $X_{Fe^{3+}}$, Fe^{3+}/(Fe^{3+} + Al); calculated from charge balance.

and X_{Mg} is always lower than in coexisting garnet (1) (Table 3). This corroborates an earlier observation that in Fe-rich rocks, such as the present ones, spinel is always less magnesian than the coexisting garnet (Sengupta *et al.*, 1991; Waters, 1991; Nichols *et al.*, 1992; Fitzsimons, 1996). The implication of this will be discussed later.

Garnet (1) in both the associations is almandine rich with significant proportions of pyrope (32–38 mol %, Table 4). Grossular and spessartine contents are always low, and together never exceed 4 mol % (Table 4). A slight increase in almandine content towards the rims (3–4 mol %) is noted at contacts with spinel. Coronal garnet has a similar composition to that of the porphyroblastic garnet rims (Table 4).

Reintegrated compositions of porphyroblastic ilmenite show significant Fe_2O_3 contents (>12 mol %, Table 5). However, granular ilmenite intergrown with coronal garnet shows lower proportions of Fe_2O_3 than spot analyses of porphyroblastic ilmenite (Table 5). The lamellar intergrowth between ilmenite and corundum suggests solubility of significant Al_2O_3 (>10 mol % calculated from image analysis) in the ilmenite structure.

Biotite included in garnet is phlogopite rich with significant TiO_2 (5·49 wt %) and F (1·38 wt %) (Table 5). Retrograde biotite has higher F (3·32 wt %) but lower TiO_2 (1·96 wt %) (Table 5).

The result of the reintegrated alkali feldspar and the antiperthite analyses by EPMA area scans are presented in Table 6. The reintegrated perthite compositions show up to 11 mol % anorthite (Table 6). The anorthite content of the plagioclase lamellae varies between 20 and 25 mol %. Porphyroblastic plagioclase shows no compositional zoning and varies in composition within a restricted range ($An_{35–30}$; Table 6).

Corundum and magnetite are nearly pure phases, but sillimanite contains up to 1·5 wt % of Fe_2O_3 (Table 5).

Table 4: Representative garnet compositions

Association:	I	I	I	I	I	I	I	I	I	II	II	II	II
Sample:	k671(c)	k671(r)	k671(cr)	k672	k673	k674	k85D	k85D1	K61	k676	k678	k680	k682
SiO_2	38·38	38·48	37·97	38·38	38·30	38·55	38·30	38·87	38·82	38·71	37·86	38·64	34·15
TiO_2	0·01	0·07	0·04		0·02		0·02		0·15	0·05	0·01	0·04	0·02
Al_2O_3	21·58	21·60	20·87	21·35	21·29	21·38	21·29	21·56	21·35	21·91	21·91	21·08	22·46
FeO	29·67	30·51	29·97	29·65	28·93	27·64	28·93	30·06	30·17	28·10	30·52	27·91	29·81
MnO	0·43	0·53	0·41	0·38	0·79	0·76	0·79	0·62	0·45	0·34	0·36	0·33	0·35
MgO	9·50	8·75	8·83	8·77	8·72	9·46	8·72	8·84	8·55	9·46	8·63	10·14	10·51
CaO	1·00	1·12	1·08	0·68	1·46	1·10	1·46	1·86	0·74	0·94	1·06	1·04	0·96
Total	100·6	101·1	99·17	99·21	99·51	98·89	99·51	101·8	100·2	99·47	100·35	99·18	98·26
Oxygen	12·00	12·00	12·00	12·00	12·00	12·00	12·00	12·00	12·00	12·00	12·00	12·00	12·00
Si	2·96	2·97	2·98	3·01	2·99	3·00	2·99	2·98	3·02	2·99	2·97	3·00	2·73
Ti									0·01				
Al	1·96	1·96	1·94	1·98	1·96	1·96	1·96	1·95	1·96	2·00	1·96	1·93	2·11
Fe^{2+}	1·92	1·97	1·97	1·94	1·89	1·80	1·89	1·93	1·97	1·82	2·00	1·81	1·99
Mn	0·03	0·03	0·03	0·02	0·05	0·05	0·05	0·04	0·03	0·03	0·02	0·02	0·02
Mg	1·09	1·00	1·03	1·03	1·01	1·10	1·04	0·97	0·99	1·09	1·00	1·17	1·25
Ca	0·08	0·09	0·09	0·08	0·12	0·09	0·12	0·15	0·09	0·08	0·09	0·08	0·08
X_{Fe}	0·61	0·63	0·63	0·63	0·63	0·59	0·61	0·62	0·64	0·60	0·64	0·59	0·61
X_{Mg}	0·35	0·32	0·33	0·33	0·33	0·36	0·33	0·31	0·32	0·36	0·32	0·37	0·37
X_{Mn}	0·01	0·01	0·01	0·01	0·01	0·02	0·02	0·01	0·01	0·01	0·01	0·01	0·01
X_{Ca}	0·03	0·03	0·03	0·03	0·04	0·03	0·04	0·05	0·03	0·03	0·03	0·03	0·02

c, core; r, rim; cr, corona; X_{Fe}, Fe/total bivalent cations, etc.

Reaction history

In association I, inclusions of biotite, sillimanite and quartz in garnet (1) suggest operation of the dehydration-melting reaction

biotite + sillimanite + quartz → garnet + liquid. (a)

Embayment of garnet (1) by lobate spinel (1) is intriguing. In domains free from complex spinel–ilmenite intergrowths, the likely reaction is

garnet + sillimanite → spinel + quartz (b1)

(Fig. 3a). This reaction proceeds to the right with rising temperature. However, the formation of spinel + ilmenite aggregates in places merits discussion. The textural and compositional data (discussed above) suggest that these aggregates are the breakdown product of a former Ti-rich spinel. As neither of the reactants in reaction (b1) can contribute Fe_2TiO_4 component, a Ti-saturating phase (such as biotite) must also be involved in these domains. It is likely that subsequent to the reaction (a) these domains were impoverished in silica and the residual biotite became more Ti rich, and ultimately reacted to form the complex Fe–Al–Ti spinel at higher temperature through the reaction

Ti-biotite + sillimanite → complex Fe–Al–Ti spinel + liquid. (b2)

Formation of coronal garnet and/or compound corona of sillimanite and garnet over the lobate spinel (Fig. 3a) suggest that reaction (b1) proceeded in the reverse direction during cooling. The free silica required for this reaction was possibly derived from the crystallization of the granitic liquid.

Intergrowth of garnet (2) and Fe_2O_3-poor granular ilmenite around Fe_2O_3-rich porphyroblastic ilmenite at the contact of plagioclase can be explained by the de-oxidation reaction of the type

Fe_2O_3-rich ilmenite + plagioclase + quartz → Fe_2O_3-poor ilmenite + garnet + O_2 (c)

(Fig. 3b). This reaction proceeds to the right during cooling and is reported from many high-grade metapelites [see Ellis & Green (1985) and Dasgupta *et al.* (1995), and references therein].

Table 5: Representative compositions of magnetite (mt), ilmenite (ilm), biotite (bt) and sillimanite (sill)

Association:	I	I	I	I	II	I	I
Sample:	k671	k672	k672	k61	k672	k671	k671
Mineral:	mt	ilm	ilm*	ilm	ilm(s)	bt(i)	bt(m)
SiO_2		0·02	0·02		36·75	37·31	38·14
TiO_2	0·03	48·19	43·02	50·27		5·49	1·96
Al_2O_3	0·18	0·05	0·04	0·03	62·77	14·86	15·41
Fe_2O_3	68·26	5·80	12·75	3·47	0·50		
Cr_2O_3	0·21	0·03	0·11	0·01	0·01	0·04	
FeO	30·97	44·00	42·42	44·36		11·67†	10·38†
MnO	0·01	0·09	0·03	0·20			
MgO	0·05	1·18	1·16	0·31		16·86	19·18
ZnO							
K_2O						10·20	10·79
Na_2O						0·19	0·19
F						1·38	3·32
Total	99·71	99·36	99·55	98·65	100·03	98·00	99·37
Oxygen	4·00	3·00	3·00	3·00	5·00	11·00	11·00
Si					1·01	2·72	2·72
Ti		0·91	0·81	0·96		0·30	0·10
Al	0·01				1·97	1·28	1·29
Fe^{3+}	1·98	0·17	0·37	0·10	0·02		
Cr	0·01						
Fe^{2+}	1·00	0·87	0·77	0·95		0·71	0·62
Mn							
Mg		0·04	0·04	0·01		1·83	2·03
Zn							
K						0·95	0·98
Na						0·03	0·03
F						0·32	0·53

*Reintegrated composition. †Total Fe as FeO.
s, symplectitic with garnet; i, included; m, matrix.

In association II, stability of corundum (1) and garnet (1) and inclusion of biotite and sillimanite in the latter suggest the reaction

$$\text{Ti-biotite} + \text{sillimanite} \rightarrow \text{garnet (1)} + \text{corundum (1)} + \text{liquid}. \quad \text{(d)}$$

However, coexistence of garnet (1), corundum (1) and spinel–ilmenite aggregates suggests the reaction of the type

$$\text{biotite} + \text{sillimanite} \rightarrow \text{garnet (1)} + \text{Ti-rich spinel} + \text{corundum (1)} + \text{liquid} \quad \text{(e)}$$

(Fig. 4b). The significant TiO_2 content in the included biotite suggests that the Ti component of the oxide aggregates was derived from biotite. This reaction was also inferred by Powers & Bohlen (1985).

The Zn-rich spinel inclusions in the cores of garnet (1) are problematic. They can form either by dehydration of staurolite or as a result of early melting of biotite in the ZnKFMASH system via the reaction

$$\text{biotite} + \text{sillimanite} + \text{quartz} \pm \text{vapour} \rightarrow \text{Zn-rich spinel} + \text{liquid}$$

(Montel *et al.*, 1986). However, the textural information is insufficient to choose between the two alternatives. Nevertheless, the presence of this type of spinel and biotite inclusions in garnet (1) suggests the reaction

$$\text{spinel} + \text{biotite} + \text{sillimanite} \rightarrow \text{garnet (1)} + \text{liquid}. \quad \text{(f)}$$

This reaction occurs at lower temperature than the biotite melting reactions (d) and (e) at pressures higher than the

Table 6: Representative feldspar compositions

Association:	I	I	I	I	I	I	I	I	I	I	II	II	II
Sample:	k671 h	k671 I	k671 R	k672 h	k672 I	k672 R	k673 R	k674 R	k85D	K85D1	K85D I	K85D h	K85D R
SiO_2	64·44	62·51	63·72	64·44	62·51	63·00	64·26	63·50	60·97	59·27	61·72	64·17	63·76
Al_2O_3	18·86	23·67	22·05	18·86	23·67	22·05	20·09	20·63	25·41	25·84	23·92	18·48	20·90
FeO	0·02	0·01		0·02	0·01		0·08	0·04	0·08	0·02	0·05	0·08	0·04
CaO	0·16	4·85	2·11	0·16	4·85	2·22	2·06	1·82	6·50	7·50	5·95	0·09	2·03
Na_2O	1·76	9·05	1·80	1·76	9·05	1·89	6·22	6·84	8·19	7·48	8·51	1·20	4·54
K_2O	14·62	0·20	12·55	14·62	0·20	12·35	5·97	6·24	0·13	0·17	0·21	15·15	8·97
Total	99·86	100·29	102·23	99·86	100·29	100·56	98·71	99·10	100·30	100·62	100·37	99·31	100·26
Oxygen	8·00	8·00	8·00	8·00	8·00	8·00	8·00	8·00	8·00	8·00	8·00	8·00	8·00
Si	2·97	2·76	2·86	2·97	2·76	2·87	2·92	2·88	2·63	2·63	2·73	2·98	2·89
Al	1·02	1·23	1·17	1·02	1·23	1·13	1·07	1·10	1·31	1·35	1·25	1·01	1·11
Fe													
Ca	0·01	0·23	0·10	0·01	0·23	0·11	0·10	0·09	0·30	0·36	0·28		0·09
Na	0·16	0·78	0·16	0·16	0·78	0·17	0·55	0·60	0·70	0·65	0·73	0·11	0·39
K	0·86	0·01	0·72	0·86	0·01	0·72	0·35	0·36	0·01	0·01	0·01	0·90	0·53
X_{Ab}	0·15	0·76	0·16	0·15	0·76	0·17	0·55	0·58	0·69	0·64	0·71	0·11	0·38
X_{Or}	0·84	0·01	0·74	0·84	0·01	0·72	0·35	0·34	0·01	0·01	0·01	0·89	0·53
X_{An}	0·01	0·23	0·10	0·01	0·23	0·11	0·10	0·08	0·30	0·35	0·28		0·09

h, host; I, lamellae; R, reintegrated composition; X_{Ab}, Na/(Na + K + Ca), etc.

KFMASH univariant reaction (Spr, Opx, Crn, Qtz) (see Fig. 6, below) and is noted in many high-grade terranes (e.g. Fitzsimons, 1996).

The coarse spinel–sillimanite intergrowth replacing garnet (1) (Fig. 4a) can be explained by the reaction

$$\text{garnet (1)} + \text{corundum (1)} \rightarrow \text{spinel} + \text{sillimanite.} \quad \text{(g)}$$

This reaction has been experimentally calibrated by Shulters & Bohlen (1989) and it proceeds to the right with rising temperature.

Evolution of the oxide aggregates

It was discussed earlier that textural features and compositional characteristics of the oxide aggregates indicate early stabilization of a Ti-rich spinel. In corundum-free aggregates, this Ti-spinel produced ilmenite$_{ss}$ ($FeTiO_3$–Fe_2O_3) and spinel$_{ss}$ ($FeAl_2O_4$–$MgAl_2O_4$–Fe_3O_4) through oxidation of the Fe_2TiO_4 component in spinel,

$$Fe_2TiO_4 + O_2 \rightarrow (FeTiO_3 + Fe_2O_3)_{ss} + Fe_3O_4 \text{ (partitioned in aluminous spinel)} \quad \text{(h)}$$

(see Haggerty, 1976).

Experimental and theoretical studies in the system Fe–Mg–Ti–Al–O (Sack & Ghiorso, 1991) indicate that spinel with >10 mol % Fe_2TiO_4 is stable only at temperatures of the order of 1000°C or more. This implies that reaction (h) occurred at very high temperature.

The ilmenite–corundum intergrowth in some of these aggregates requires an additional reaction of the type

$$FeAl_2O_4 + O_2 \leftrightarrow Fe_3O_4 \text{ (partitioned in spinel)} + Al_2O_3 \text{ (in ilmenite)} \quad \text{(i)}$$

(Fig. 4e).

The presence of abundant corundum lamellae in ilmenite indicates significant solubility of Al_2O_3 in ilmenite. Experimental data of Hauck (1981) show that only at temperatures higher than 1100°C can the ilmenite structure incorporate a substantial amount (>10 mol %) of Al_2O_3. Separate rimming of ilmenite and spinel by coronal garnet (Fig. 4f) suggests that formation of the latter mineral occurred subsequent to the reactions (h) and (i).

The development of magnetite lamellae of different thickness in spinel and Ti-haematite lamellae in ilmenite (Fig. 4c and d) indicate progressive supersaturation in Fe_3O_4-rich spinel and Fe_2O_3-rich ilmenite solid solutions during cooling [see Haggerty (1976)]. Available experimental data and theoretical analysis of the spinel$_{ss}$

($FeAl_2O_4$–$MgAl_2O_4$–Fe_3O_4) suggest that unmixing of spinel$_{ss}$ (with up to 15 mol % magnetite) occurred at T < 800°C [see Nell *et al.* (1989)]. Formation of discrete corundum laths in spinel and the occurrence of magnetite granules along the contact (Fig. 4c) suggest that reaction (i) also occurred at lower temperatures subsequent to the separation of ilmenite from spinel (Clarke *et al.*, 1989).

Petrogenetic grid

The metamorphic evolution of the studied metapelitic rocks can be portrayed in a petrogenetic grid in the system KFMASH with TiO_2, Fe_2O_3, ZnO and F as extra components. Considering the fact that the Fe–Ti–Al oxide aggregates are products of oxy-exsolution of Fe_2TiO_4-rich spinel, these extra components do not form any new phase. Hence, the effect of incorporation of these non-KFMASH components will only be to increase the variance of the KFMASH assemblages. Excepting the one reported by Srogi *et al.* (1993), all other published petrogenetic grids for the KFMASH system or its subsystem FMAS consider either corundum- or quartz-bearing assemblages and hence are not suitable for the present study (see Grant & Frost, 1990; Hensen & Harley, 1990; Dasgupta *et al.*, 1995). The petrogenetic grid of Srogi *et al.* (1993), on the other hand, does not include high-temperature phase relations. For this reason, a new petrogenetic grid has been constructed combining the available experimental data and the constraints imposed by the natural assemblages (Fig. 5).

We begin our analysis in the simplified KFMASH system and the effects of the non-KFMASH components will be discussed subsequently. Textural relations suggest that the early melting reactions with biotite evolved in the KFMASH system. Following the elimination of biotite and extraction of the melt, the subsequent mineral reactions evolved in the simplified FMAS sub-system. For quartz-bearing assemblages, the geometrical relations in the KFMASH and FMAS systems and their interrelationships have been elegantly presented by Hensen & Harley (1990). The topology presented in Fig. 5, although broadly similar to that of Hensen & Harley (1990), differs in the relative position of garnet and spinel in some of the reactions. Hensen & Harley (1990) considered the FMAS topology of Hensen (1986), which is valid for X_{Mg}(Spinel) > X_{Mg}(Garnet). However, in Fe-rich bulk compositions, such as the present one, the relationship is reversed (Grant & Frost, 1990; Clarke & Powell, 1991; Sengupta *et al.*, 1991; Waters, 1991; Fitzsimons, 1996; references cited therein). As a consequence, garnet and spinel change sides in some univariant reactions to maintain reaction stoichiometry. Waters (1991) showed that in the simple FMAS system (i.e. the biotite-free portion of Fig. 5) spinel + cordierite + quartz will be stabilized only in very iron-rich bulk compositions and cordierite with X_{Mg} up to 0·4 can coexist with spinel. However, in most of the natural spinel + cordierite-bearing assemblages, the X_{Mg} of cordierite exceeds 0·6 (Waters, 1991). Waters explained this anomaly by the up-pressure shift of the reaction spinel + cordierite + quartz ↔ garnet + sillimanite because of incorporation of non-KFMASH components such as Fe_2O_3, TiO_2, and ZnO in spinel. Geometric relations further indicate that a topological inversion would occur when such a shift of spinel-bearing equilibria causes the invariant point [Spl, Bt, Crn] to lie within the stability field of spinel (Hensen & Harley, 1990; D. J. Waters, personal communication, 1998). This will generate the new invariant points [Opx, Crn, Bt], [Spr, Crn, Bt], [Grt, Crn, Bt] and [Crd, Crn, Bt]. However, the [Spl, Spr, Crn] invariant point of Hensen & Harley (1990) will remain essentially unaltered. This is shown in Fig. 5, where the last two invariant points are omitted for the sake of clarity. Experimental investigations of Annersten & Seifert (1981) showed that the assemblage spinel–orthopyroxene–sillimanite–quartz, which is the key assemblage for the inverted topology, is stabilized as a result of significant incorporation of Fe_3O_4 at high fO_2. This, together with the observation that this four-phase assemblage mostly occurs in high-fO_2 granulites, led Hensen (1986) to conclude that fO_2 is the only controlling factor for the topological inversion. Subsequent work of Sengupta *et al.* (1991), Waters (1991), Nichols *et al.* (1992) and Fitzsimons (1996), although supporting the contention of Hensen (1986), also emphasizes the role of other non-FMA components such as ZnO and TiO_2 in stabilizing the spinel-bearing assemblages and consequent topological inversion. Using the internally consistent data set of Holland & Powell (1990), D. J. Waters (personal communication, 1998) showed that spinel should contain nearly 20 mol % non-KFMASH components to cause the topological inversion and that the absolute P–T positions of [Spr, Crn, Bt] and [Crd, Crn, Bt] are determined by the amount of non-FMA components in spinel. With increasing impurities, the sapphirine- and cordierite-absent invariant points would move towards [Spl, Spr, Crn], thereby causing contraction of the triangular area bounded by these invariant points (Fig. 5). Incorporation of F and Ti in biotite would further shrink this triangle, but towards higher temperatures (Fig. 5). We have chosen the inverted topology because of the presence of significant non-KFMASH components in early spinel and the high fO_2 conditions (indicated by the presence of ferrian ilmenite). To explain the corundum-bearing reactions, another invariant point [Spr, Qtz, Opx] is created (Fig. 6). The geometry around this invariant point is similar to that of Srogi *et al.* (1993), except for some spinel–garnet equilibria for reasons stated above. The topological constraints of Fig. 6 indicate that

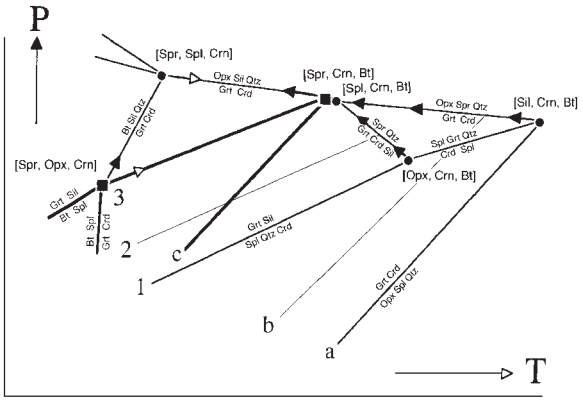

Fig. 5. Schematic petrogenetic grid in the system KFMASH. Filled circles and thin lines are the invariant points and related univariant reactions similar to the 'low fO_2' grid of Hensen (1986). [Note that Spl and Grt change their side in some of the reactions (see text).] Filled squares and thick lines are the invariant points and the related univariant reactions in the inverted topology [similar to 'high fO_2' grid of Hensen (1986)]. a–b–c , 1–2–3 and solid arrowheads indicate the shifts of some 'low fO_2' reactions [e.g. (Sil, Crn, Spr, Bt) and (Opx, Crn, Spr, Bt)] as a result of presence of non-FMAS components in spinel (see text). Open arrowhead indicates the displacement of the reactions for Ti and F in biotite (see text). Some uni- and invariant reactions are omitted for clarity. Mineral abbreviations are after Kretz (1983).

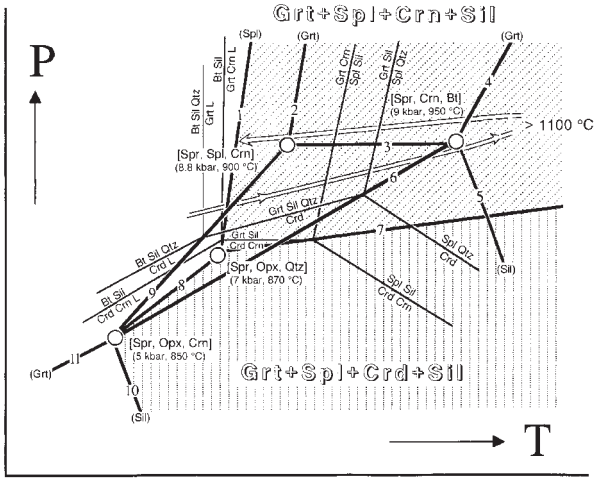

Fig. 6. Schematic partial petrogenetic grid in the system KFMASH involving Qtz and Crn. The thick and thin lines are the univariant and some bivariant reactions, respectively. The stability fields of the assemblages Grt + Spl + Crn + Sil and Grt + Spl + Crd + Sil are shaded. The *P–T* coordinates of the Crn absent invariant points are taken from Dasgupta *et al.* (1995), and the same coordinate for [Spr, Opx, Qtz] has been deduced in this study (see text). The pressure–temperature trajectory constrained from the textural relations is shown by thick and hollow line with arrowhead. Univariant reactions: 1, Bt + Sill ↔ Grt + Cd + Crn + L; 2, Bt + Sill + Q ↔ Opx + Cd + L; 3, Opx + Sill + Q ↔ Gt + Cd; 4, Sp + Cd + Q ↔ Opx + Sill; 5, Gt + Cd ↔ Sp + Opx + Q; 6, Gt + Sill ↔ Cd + Sp + Q; 7, Gt + Sill↔ Sp + Cd + Crn; 8, Bt + Gt + Sill ↔ Sp + Cd + L; 9, Bt + Sill + Q ↔ Gt + Cd + L; 10, Bt + Sp + Q ↔ Gt + Cd + L; 11, Bt + Sill + Q ↔ Sp + Cd + L.

this invariant point will lie in the triangular area defined by the three corundum-absent invariant points and should be bounded by the (Opx) and (Sill) absent reactions emanating from the invariant point [Spr, Spl, Crn]. Also shown in Fig. 6 are some of the bivariant reactions relevant to this study.

In the *P–T* region of biotite-dehydration melting, K-feldspar can be either a reactant or a product depending upon the H_2O/K_2O ratio in the melt and biotite (Carrington & Watt, 1995). If we consider the F contents of biotite inclusions to be representative of compositions at the time of melting, it is likely that the H_2O/K_2O ratio of biotite was higher than that of the coexisting melt. This places K-feldspar on the reactant side of the dehydration melting reactions. However, the topology presented in Fig. 6 would change only marginally with a change of side for K-feldspar in the melting reactions (Fitzsimons, 1996).

The thermobaric evolution of the study assemblages can be better explained if the *P–T* coordinates of the invariant points shown in Fig. 6 are available. The experimental data of Carrington & Harley (1995) for the system KFMASH tightly constrains the *P–T* coordinates of [Spr, Spl, Crn, Bt] at 9 $\pm$ 0·5 kbar and 900°C, which is also corroborated by the thermodynamic analysis of Holland *et al.* (1996) (their [Os] invariant point). The presence of Ti and F in biotite would shift the invariant point towards higher temperature (Fig. 5). Considering the TiO_2 and F contents of biotite inclusions (Table 5), a minimum of 30°C up-temperature shift of this invariant point is expected from the experimental data of Hensen & Osanai (1994). On the basis of *P–T* estimates of natural assemblages, Dasgupta *et al.* (1995) showed that the invariant points [Opx, Spr] (equivalent to [Opx, Spr, Crn] in Fig. 6) and [Spr, Bt] (equivalent to [Spr, Bt, Crn] in Fig. 6) occur at 5 $\pm$ 1 kbar, 750–850°C and ~9 kbar and 950°C, respectively. Using the thermodynamic data of Holland *et al.* (1996), D. J. Waters (personal communication, 1998) calculated the *P–T* coordinates of these two invariant points with 20 mol % of non-aluminous components in spinel. Although the calculated *P–T* coordinates of [Spr, Crn, Bt] match perfectly with those of Dasgupta *et al.* (1995), the invariant point [Opx, Spr, Crn] is placed at nearly the same pressure but at a temperature ~100°C lower (Fig. 5). However, if the shift of the biotite-melting reaction (Spr, Opx, Crn, Spl) for these non-aluminous components is calculated using the experimentally determined ones of Carrington & Harley (1995), the resultant *P–T* coordinates of [Spr, Opx, Crn] match perfectly with those of Dasgupta *et al.* (1995). Holland *et al.* (1996) also argued that the reactions involving biotite calculated from their data set are always placed at temperatures 80–100°C lower than the experimentally determined positions of Carrington & Harley (1995), and attributed this discrepancy to the poorly

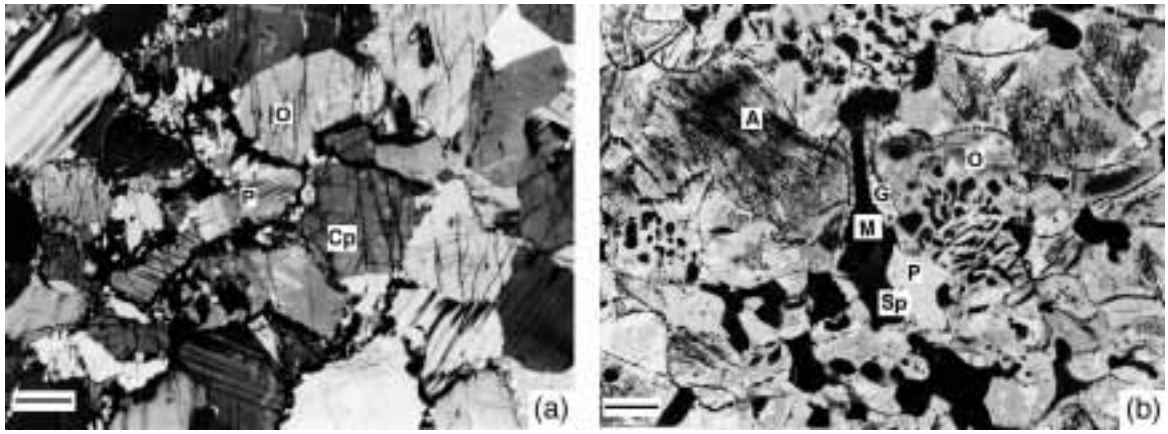

Fig. 7. Photomicrographs illustrating reaction textures in mafic–ultramafic rocks. (a) Thin garnet corona (black) along the contacts of orthopyroxene (O), clinopyroxene (Cp) and plagioclase (P) in gabbronorite. Bar represents 200 μm. (b) Coarse spinel (Sp) showing granular exsolution of magnetite (M) and forming a granoblastic mosaic with orthopyroxene (O) and plagioclase (P). [Note the symplectitic intergrowth of orthopyroxene and the secondary spinel. Also note the thin garnet (G) corona on spinel.] Secondary amphibole (A) replacing orthopyroxene and plagioclase. Fine opaque phases in amphibole are ilmenite and magnetite. Bar represents 200 μm.

constrained melt parameters used in their data set. In view of this, we have adopted the P–T coordinates of these invariant points from Dasgupta *et al.* (1995).

The $P_{[Spr,Opx,Qtz]}$ can be estimated using the topological constraints $P_{[Opx,Spr,Crn]} < P_{[Spr,Opx,Qtz]} < P_{[Spl,Spr,Crn]}$. The P coordinates of the bounding invariant points give a large pressure bracket of 5–9 kbar. However, for spinel containing >20 mol % non-aluminous components and biotite with appreciable Ti and F, the pressure bracket will be narrower. Powers & Bohlen (1985) and Srogi *et al.* (1993) described an assemblage that equilibrated close to $P_{[Opx,Spr,Crn]}$. Geobarometry in these areas indicates $P \sim 7 \pm 1$ kbar. Recently, Dasgupta *et al.* (1997) have reported the cordierite–corundum–spinel–sillimanite assemblage, which lies below the biotite-absent univariant curve emanating from this invariant point (Fig. 6). Those workers estimated a pressure of 7 kbar using different barometric estimates. Considering the nearly flat slope of the biotite-absent reaction and barometric estimates for the above areas, the $P_{[Spr,Opx,Crn]}$ is placed at 7 ± 1 kbar.

Several important points emerge from the topology presented in Fig. 6:

(1) dehydration melting of biotite + sillimanite + quartz can produce spinel + cordierite or garnet + cordierite depending on the depth of melting, i.e. at pressures lower and higher than $P_{[Spr,Opx,Crn]}$, respectively. This is consistent with the widespread occurrence of spinel + cordierite in low-pressure contact aureoles and of garnet + cordierite-bearing assemblages in medium- and high-pressure (>5 kbar) regionally metamorphosed pelites (Grant & Frost, 1990; Harley *et al.*, 1990; Dasgupta *et al.*, 1995; Fitzsimons, 1996; references therein).

(2) In quartz-undersaturated sillimanite-rich metapelite (with Ti- and F-rich biotite), complete elimination of biotite would indicate very high temperatures, i.e. above 900°C.

(3) In silica-undersaturated iron-rich metapelites, corundum-bearing assemblages are potentially valuable depth indicators. The assemblage garnet + corundum + spinel + sillimanite occurs exclusively at pressures $>P_{[Spr,Opx,Qtz]}$ and is only expected in deep crustal rocks, whereas the cordierite + corundum + sillimanite + spinel-bearing assemblages occur at lower pressures. This is consistent with the preponderance of the latter assemblage in upper- and mid-crustal contact aureoles [reviewed by Barton *et al.* (1991) and Dasgupta *et al.* (1997)].

The mineral assemblages and the inferred mineral reactions in the studied rocks can now be interpreted in terms of this petrogenetic grid. Textural relations presented above suggest that biotite in both the associations was eliminated through a number of dehydration-melting equilibria within the temperature interval of $T_{[Spr,Opx,Crn]}$ and $T_{[Spr,Opx,Qtz]}$ (Fig. 6). The appreciable amount of Fe_2TiO_4 (>19 mol %, Table 3) in the pristine spinel indicates that the peak metamorphic assemblages were stabilized beyond $T_{[Spr,Crn,Bt]}$ (i.e. >950°C). Non-appearance of other characteristic high-temperature assemblages such as sapphirine + quartz, osumilite + garnet ± sapphirine ± orthopyroxene can be attributed to the Fe-rich bulk composition of the rocks (Hensen & Harley, 1990). The occurrence of corundum + garnet + sillimanite + spinel and absence of cordierite in the quartz-undersaturated association II indicate that the prograde reactions occurred at high

pressures, i.e. $P > P_{[Spr,Opx,Qtz]}$. Textural features further suggest that all the biotite-absent reactions were intersected twice from opposite directions, i.e. during the prograde and retrograde stages of metamorphism. In the absence of orthopyroxene and sapphirine no upper pressure limit can be constrained from the petrogenetic grid. However, the geobarometric estimates, discussed below, indicate that cooling occurred at pressures above $P_{[Spr,Bt,Crn]}$. Taken together, all this evidence indicates an anticlockwise heating–cooling path at pressures above $P_{[Spr,Opx,Qtz]}$ (Fig. 6).

Geothermobarometry

The absence of orthopyroxene and cordierite excludes application of most of the cation-exchange thermometers in the study rocks. However, oxide and feldspar thermometers can be applied to constrain the peak temperature of metamorphism. The reintegrated spinel compositions (with >19 mol % Fe_2TiO_4) requires temperatures in excess of 1000°C (Sack & Ghiorso, 1991). This is a conservative estimate as the aggregates with minimum modal ilmenite were considered. Temperatures in excess of 1000°C are also required to dissolve significant amounts of Al_2O_3 (10 mol % or more) in the ilmenite structure (Hauck, 1981). Bulk compositions of feldspars when projected on the ternary feldspar isotherms at 10 kbar of Hayob *et al.* (1989) indicate temperatures in the range of 950–1000°C. These too are conservative estimates in view of the likely partitioning of some Ca from alkali feldspar to porphyroblastic plagioclase during cooling [see Kroll *et al.* (1992)]. Such an extreme temperature is consistent with the predicted temperature (>900°C) for the instability of the assemblage Ti-rich biotite + sillimanite ± quartz from the petrogenetic grid (Fig. 6). Host–lamellae pairs in alkali feldspars yield distinctly lower values (650–700°C), which are obviously cooling temperatures.

Peak metamorphic pressure, on the other hand, can be estimated using the pressure-sensitive equilibria involving garnet–plagioclase–sillimanite–quartz (GPSQ, Koziol & Newton, 1988), garnet–corundum–spinel–sillimanite (GCSpS, Shulters & Bohlen, 1989), and garnet–sillimanite–spinel–quartz (GSSpQ, Bohlen *et al.*, 1986). The spinel-bearing equilibria are sensitive to the input spinel composition and temperature [see Shulters & Bohlen (1989)]. To obtain a conservative pressure estimate, we have used spot analyses of spinel and 950°C (the minimum estimates of the peak temperature). Application of the GPSQ equilibrium to the studied rocks is fraught with uncertainties inherent in the low grossular content of garnet (Table 4). Notwithstanding the uncertainties associated with these barometers, the three equilibria yield metamorphic pressures mostly in the range of 9–10 kbar (Table 7). These pressure values are consistent with the constraints imposed by the petrogenetic grid (i.e. stability of garnet + corundum and absence of cordierite in association II). The estimates match well with the results from the more precise GOPS and GCPS barometry in the enclosing mafic rocks (Table 7).

P–T HISTORY OF THE LAYERED BASIC INTRUSION

The mafic members of the complex are olivine- to quartz-normative low-K tholeiites with *mg*-number varying from 30 to 74. Magnesian varieties are olivine-normative (1–12% normative olivine), whereas the Fe-rich rocks are quartz-normative (4–6% normative quartz). The compositional range overlaps with the experimental run composition (No. R 698) of Irving (1974) and the tholeiitic composition of Green & Ringwood (1967). This allows direct application of their experimental phase diagrams to this rock suite. Representative compositions of the different phases in the members of the layered complex are presented in Tables 2 and 7. The mafic rocks consist of orthopyroxene, clinopyroxene, highly calcic plagioclase and ilmenite. Olivine is conspicuously absent and coronal garnet developed only in the Fe-rich rocks. Orthopyroxene and clinopyroxene often contain coarse to fine (100) lamellae of Ca-rich and Ca-poor pyroxene, respectively. Reintegrated pyroxene compositions yield temperatures of 1000–1100°C when plotted on the projected isotherm of Davidson & Lindsley (1989). The calculated temperatures are also consistent with the solidus temperature of tholeiitic magma at 8–10 kbar (Green & Ringwood, 1967; Irving, 1974). Non-appearance of olivine even in olivine-normative rocks indicates that the depth of emplacement of the magma was higher than the stability field of olivine + plagioclase. The phase diagram of Irving (1974) suggests a pressure of magmatic crystallization above 6 kbar at 1100°C. However, non-appearance of garnet constrains an upper pressure limit of 11 kbar at the same temperature (Green & Ringwood, 1967; Irving, 1974). In Fe-rich rocks, thin coronas of garnet or garnet–quartz symplectite locally occur along the contacts of pyroxene–plagioclase–ilmenite (Fig. 7a). This garnet is likely to have formed during subsolidus, near-isobaric cooling of the rocks [see Ellis & Green (1985)].

Further evidence in support of such deep-level intrusion comes from the mineralogy of the layers and/or xenoliths of clinopyroxenite and hercynite-bearing orthopyroxenite. Clinopyroxenite is composed dominantly of cumulus clinopyroxene with extremely calcic plagioclase and few grains of orthopyroxene as intercumulus phases. This suggests crystallization from the enclosing mafic to

Table 7: Results of thermobarometry

	Opx	Cpx	Garnet			Spl	Plg	A*†		B†		C*†		D†	E†	F†	G	H
	X_{Fe}	X_{Fe}	X_{Fe}	X_{Mg}	X_{Ca}	X_{Mg}	X_{An}	P_{Fe}	P_{Mg}	P_{Fe}	P_{Mg}	P_{Fe}	P_{Mg}					
k122	0·55	0·37	0·61	0·10	0·26		0·57	6·5	10·7	8·1	8·5	8·3	9·1				720°C	670°C
k176		0·41	0·61	0·10	0·26		0·50					8·3	9·3					700°C
k176a	0·38		0·61	0·08	0·27		0·56	6·3	10·9	7·9	8·2						720°C	
k671			0·63	0·32	0·03	0·39								9·7				
k672			0·63	0·32	0·03	0·36								9·4				
k673			0·63	0·33	0·04	0·36								9·5				
k674			0·59	0·36	0·03	0·36								8·9				
k678			0·64	0·32	0·03	0·36									10·1			
k680			0·59	0·37	0·03	0·38									10·0			
k682			0·61	0·37	0·02	0·41									11·0			
k85D			0·61	0·33	0·04		0·30									9·9		
k85D1			0·62	0·31	0·05		0·35									9·7		

A, Perkins & Chipera (1985); B, Bhattacharya *et al.* (1991); C, Moecher *et al.* (1988); D, Bohlen *et al.* (1986); E, Shulters & Bohlen (1989); F, Koziol & Newton (1988); G, Lee & Ganguly (1988); H, Ellis & Green (1979).
*Pressures (in kbar) calculated with the following activity models: garnet (Anovitz & Essene, 1987), plagioclase (Newton, 1983) and pyroxenes (Wood & Banno, 1973).
†Pressures calculated at 700°C (other pressures are calculated at 950°C; see text).

anorthositic melt of clinopyroxene followed by orthopyroxene and plagioclase. Available experimental data on basaltic rocks of varied bulk compositions suggest that clinopyroxene can be the sole liquidus phase only at pressures >8 kbar (e.g. Fram & Longhi, 1992).

The hercynite-bearing orthopyroxenite is dominated by spinel and orthopyroxene with one or more of the phases plagioclase, clinopyroxene or olivine. Olivine and plagioclase never coexist and amphibole is the common retrograde phase that replaces the pyroxenes. Spinel occurs in two modes. Coarse spinel forms granoblastic mosaics with orthopyroxene. This spinel shows granular exsolution of magnetite (Fig. 7b). The other type of spinel forms myrmekitic intergrowths with orthopyroxene and, less frequently, with clinopyroxene (Fig. 7b). Thin rims of garnet are locally present around pyroxenes, hercynite and plagioclase. Symplectitic intergrowths of orthopyroxene and hercynite similar to this are common in many lower-crustal xenoliths and are interpreted to have formed by either of the two processes: (a) replacement of olivine + plagioclase or (b) direct crystallization of aluminous pyroxene and subsequent subsolidus exsolution in the spinel peridotite–gabbro stability field (e.g. Green & Ringwood, 1967; Ellis & Green, 1985; Ballhaus & Berry, 1991; Dasgupta *et al.*, 1993). Mutual exclusion of olivine and plagioclase tends to support the second alternative. The mineralogical evolution can be presented schematically as follows: Stage 1: Al-Opx(1) → Al-Opx(2) + Spinel; Stage 2: Al-Opx(2) → Garnet. The estimated P–T conditions of the garnet-bearing mafic rocks cluster around 8–9 kbar and 670–720°C (Table 7). The temperature estimates are obviously cooling temperatures reflecting the blocking of Fe–Mg exchange between garnet and pyroxenes [see Ellis & Green (1985)]. Distinctly lower pressures (4–5 kbar at 700°C) are obtained from the alumina solubility in orthopyroxene coexisting with garnet in the hercynite-bearing orthopyroxenite (Harley, 1984). Fitzsimons & Harley (1994) showed that the formulation of Harley (1984) is strongly sensitive to retrograde Fe–Mg resetting, which often leads to underestimation of the equilibrium pressure in the natural assemblages.

Summarizing, the mineralogical and phase compositional attributes constrain the emplacement and fractionation of the layered magmatic suite to have occurred above 8 kbar and at temperatures ≥1100°C. Subsequent near-isobaric cooling produced coronal garnet in the Fe-rich mafic rocks and exsolution of spinel from the aluminous pyroxene in the hercynite-bearing orthopyroxenite.

DISCUSSION

It is evident from the petrological analysis of the khondalites that biotite in these rocks was completely eliminated

through a number of dehydration-melting equilibria leading either to stabilization of garnet ± sillimanite (association I) or garnet + corundum (association II) in centimetre-scale domains. Hence, the occurrence of quartz- and corundum-bearing assemblages in this area cannot be explained by differential thermal conditions as invoked by many workers (e.g. Srogi *et al.*, 1993). Further, similar compositions of garnet and spinel in the two associations suggest that the bulk Fe/Mg ratio was also not the deciding factor. Fitzsimons (1996) argued that dehydration-melting in sillimanite-saturated pelitic rocks can eliminate either quartz or biotite depending on the bulk $SiO_2/(FeO + MgO)$ ratio, which is dictated by the volume ratio of quartz/biotite. In view of this, it seems likely that the protolith of association II had a higher biotite/quartz ratio [hence, lower $SiO_2/(FeO + MgO)$] than association I and, as a consequence, quartz was eliminated before biotite in the former, after the first stage of dehydration-melting [i.e. reaction (a)]. Following dehydration-melting of biotite + sillimanite, porphyroblastic corundum was stabilized in association II. Subsequent prograde reactions stabilized spinel + quartz and spinel + sillimanite in corundum-free and corundum-bearing associations, respectively.

'Fossil' oxide and feldspar thermometry together with reintegration of the complex intergrowths among Fe–Ti–Al oxide phases indicates ultra-high temperatures of metamorphism similar to the solidi of tholeiitic melts (>1000°C). Such an extreme temperature of metamorphism is expected only in the presence of an advective heat supply [reviewed by Harley (1989, 1992)]. In view of the intimate association of the studied khondalites with the voluminous mafic–ultramafic layered complex, we are tempted to conclude that the required thermal input for the UHT metamorphism was supplied by the crystallization of the enclosing basic melt (Wells, 1980; Bohlen, 1987; Hensen & Harley, 1990; Waters, 1991). The estimated emplacement depth of the igneous complex, together with the topological constraints on the khondalite assemblages, indicates that the basic magma was emplaced and interacted with the metapelites in the lower crust (>8 kbar). Subsequently, both the UHT khondalites and the igneous rock suite cooled near-isobarically to 700°C (at 9–10 kbar) during which time coronal garnet and complex oxide–oxide and oxide–silicate intergrowths were formed. The prograde and retrograde reactions deduced from the 'frozen in' reaction textures and the topological constraints suggest that the mineralogical evolution in the khondalites occurred along an 'anticlockwise heating–cooling' P–T trajectory (Fig. 6). The ubiquitous occurrence of sillimanite and spinel (both as inclusions and matrix phases), together with the complete absence of any early high-pressure relics, further corroborates this contention [see Hensen & Harley (1990)]. The thermal perturbation required for the UHT metamorphism was likely to be caused by the crystallization of the basic liquid parental to the layered complex. Harley (1989) showed that an anticlockwise P–T trajectory is the normal consequence for rocks residing within and below the magma accretion zone. This study area thus joins a few regional UHT granulite occurrences that demonstrate the accretion of voluminous basic magma, concomitant UHT metamorphism and crustal anatexis followed by near-isobaric cooling in the lower crust [reviewed by Harley (1989) and Barton *et al.* (1991)].

Comparison with the northern sector of the Eastern Ghats Belt and East Antarctica

Available petrological information from several parts in the northern sector of the Eastern Ghats Belt indicates at least two phases of granulite facies metamorphism [reviewed by Dasgupta & Sengupta (1995)]. The earlier one is characterized by UHT metamorphism followed by near-isobaric cooling. Relics of prograde metamorphism, albeit documented from only few places, suggest that the UHT metamorphism occurred on an anticlockwise P–T trajectory (Sengupta *et al.*, 1990; Dasgupta *et al.*, 1995; Mukhopadhyay & Bhattacharya, 1997). On the other hand, Lal *et al.* (1987), interpreting the reaction textures of a suite of Mg–Al granulites from the Paderu area, construed a moderate to steeply decompressive retrograde path from the peak temperature. Although the rocks do not preserve any information on the prograde path, those workers preferred a 'clockwise' path on the basis of the retrograde P–T trajectory. However, the reaction textures of Lal *et al.* (1987) have been reinterpreted by Harley (1989) and Pal & Bose (1997), who postulated a near-isobaric cooling from the peak temperature followed by a steeply decompressive P–T path. Interpreting the reaction textures from the granulites of the Chilka Lake area, Eastern Ghats Belt, Sen *et al.* (1995) showed a complex retrograde P–T trajectory with a steep decompression from the peak temperature followed by near-isobaric cooling. Although some decompression from the peak temperature is also possible along an anticlockwise P–T trajectory [see path 6 in fig. 3D of Harley (1989)], in the absence of any relics of prograde metamorphism, the nature of the P–T evolution in the Chilka Lake area remains unclear.

Except for the depth of metamorphism, the metamorphic history construed in this work has striking resemblance to that of the Ongole area (Dasgupta *et al.*, 1997) in the southern sector of the belt (Fig. 1). These P–T paths are very similar to the first granulite facies event recorded in most places in the northern sector. However, in the absence of definitive geochronological support, their temporal equivalence cannot be invoked at the present state of information. Subsequent to this

event, the rocks in the northern sector witnessed another granulite facies metamorphism at distinctly lower peak metamorphic temperature (750–850°C at ~8 kbar), followed by a steeply decompressive retrograde *P–T* segment [650–700°C and 4–5 kbar; reviewed by Dasgupta & Sengupta (1995) and schematically shown in Fig. 8]. In fact, this is the more dominant petrological overprint in the northern sector, and has thoroughly reworked the older near-isobarically cooled granulites [see Dasgupta & Sengupta (1995)]. The available geochronological data indicate the last granulite facies metamorphism to be at ~1000 Ma in this sector. These data include the U–Pb cooling ages of zircon, allanite, monazite, perrierite and titanite (Grew & Manton, 1986; Aftalion *et al.*, 1988; Paul *et al.*, 1990; Mezger *et al.*, 1996; Mezger & Cosca, 1999). Except for zircon, the blocking temperatures of all other dated minerals are lower than the peak metamorphic temperature of the second granulite facies event [see Mezger *et al.* (1996)]. The ~1000 Ma zircons were also collected from granitoid rocks that intruded the older granulite basement (Grew & Manton, 1986; Aftalion *et al.*, 1988; Paul *et al.*, 1990). The only exception to this is the 863 Ma discordant U–Pb age of a titanite from the Rajamundry area (Mezger & Cosca, 1999). This age is distinctly younger than the ~1000 Ma 'Rayner Orogeny'. Mezger & Cosca (1999) have argued that the titanite from the northern sector shows resetting to various degrees subsequent to the ~1000 Ma metamorphism, and have attributed this discordance to a late thermal overprint at ~550 Ma. The effect of this last event was not strong enough to completely homogenize the ~1000 Ma memory of the titanite. In view of these observations it is reasonable to conclude that the second granulite facies event in the northern sector is characterized by a steeply decompressive retrograde *P–T* path that occurred at ~1000 Ma. Therefore, this second granulite facies event in the northern sector of the Eastern Ghats Belt has remarkable similarity to the Rayner complex exposed along the McRobertson Land and Kemp coast of East Antarctica (see Fig. 8). In contrast to the northern sector, a decompressive metamorphic overprint is, so far, not recognized in the southern sector, although only a few areas have been investigated (Fig. 8). The available U–Pb cooling ages of minerals also indicate no significant high-grade metamorphic event subsequent to ~1600 Ma (in Kondapalle) and ~1300 Ma (in Ongole) except for late shear zones. These narrow shear zones record a mild Grenvillian thermal imprint that could reset the ^{40}Ar–^{39}Ar radioclock (1100 Ma) of amphibole but not the U–Pb systematics of allanite and monazite. Geochemical data are meagre in the southern sector. However, on the basis of the available petrological features together with the absence of a Grenvillian granulite facies event in the two areas of the southern sector, it is tempting to compare the metamorphic history of this segment of the Eastern Ghats Belt with the Napier complex of East Antarctica. This would provide an important petrological constraint to delineate the Napier–Rayner terrane boundary in the Eastern Ghats Belt provided that the former terrane is correlatable with the latter belt.

The Napier–Rayner boundary in the Eastern Ghats—a metamorphic perspective

In East Antarctica, the ~1000 Ma Rayner complex (along the McRobertson Land and Kemp coast) with its characteristic decompressive *P–T* path and moderate *P–T* conditions (7–8 kbar, ~800°C) contrasts sharply with the Archaean Napier complex with its distinctive UHT metamorphism and retrograde near-isobaric cooling *P–T* path [reviewed by Harley & Hensen (1990)]. Thus, the Napier–Rayner boundary (N–R) near the Edward VIII Gulf can be viewed as a boundary separating two blocks with contrasting thermal histories and retrograde *P–T* paths. This boundary plays an important role in the assembly of the East Gondwana supercontinent. Recognizing the importance of locating the continuation of the N–R boundary in the Eastern Ghats Belt, several attempts have been made in this direction (e.g. Grew *et al.*, 1988; Chetty, 1995). The peak thermal conditions and the retrograde *P–T* loops are considered to be important characteristics in identifying the Napier and Rayner terranes, and hence, delineating their boundary in East Antarctica (Harley & Hensen, 1990). None of these studies, however, considered using the metamorphic impress to identify this boundary in the Eastern Ghats Belt. Grew & Manton (1986) first documented an ~1000 Ma age for the metamorphic and magmatic events in the Anakapalle area, Eastern Ghats Belt (Fig. 8). Combining these age data with the ~1900 Ma allanite age of Vinogradov *et al.* (1964) from an unmetamorphosed apatite–magnetite vein from the adjoining Kashipatnam area, Grew *et al.* (1988) construed the N–R boundary to pass south of Anakapalle (Fig. 8). Recently, Kovach *et al.* (1997) and Mezger & Cosca (1999) redetermined the age of the same vein (dating the zircon) and obtained a Pan-African age (~500 Ma). Chetty (1995) delineated this boundary to the north of Anakapalle on the basis of intercontinental lineament correlations (Fig. 8). However, there is no lithological break across his inferred boundary, and this, together with the Grenvillian age of metamorphism of granulites at Anakapalle (Grew & Manton, 1986), argues against such a correlation (see Fig. 8). Recently, Dasgupta *et al.* (1995) documented polyphase granulite facies metamorphism in which the last event shows a steep decompression from 8 kbar, 800°C to 5 kbar, 650°C from the Rajamundry area lying north of but close to the Godavari rift (Fig. 8).

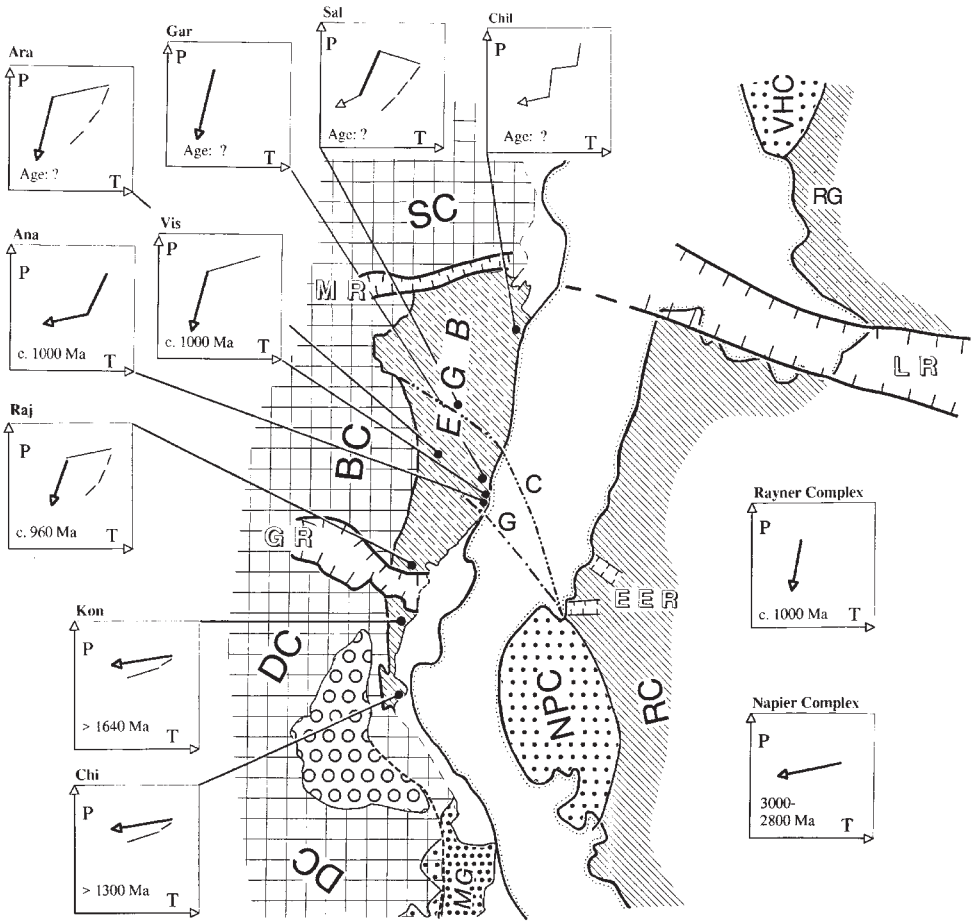

Fig. 8. Metamorphic pressure–temperature trajectories of different domains in the Eastern Ghats Belt of India and Enderby Land, East Antarctica. The last granulite facies event in the different domains of both continents is in bold. The quoted ages are related to these last events (see text). The similarity in the metamorphic *P–T* histories of the northern and southern segments of the Eastern Ghats Belt to those of the Napier and Rayner complexes, respectively, should be noted. Thin broken lines are the proposed extension of the Napier–Rayner boundary into the Eastern Ghats Belt: C, Chetty (1995); G, Grew *et al.* (1988). Ara, Araku–Anatagiri (Sengupta *et al.*, 1990); Gar, Garbhum (Dasgupta *et al.*, 1992); Sal, Salur (Mukhopadhyay & Bhattacharya, 1997); Chil, Chilka Lake (Sen *et al.*, 1995); Ana, Anakapalle (Dasgupta *et al.*, 1993); Vis, Visakhapatnam (Kamineni & Rao, 1988); Raj, Rajamundri (Dasgupta *et al.*, 1995); Chi, Chimakurthi (Ongole) (Dasgupta *et al.*, 1997); Kon, Kondapalle (this work). All other abbreviations are as in Fig. 1.

Available geochronological data (discussed above) indicate the last high-grade metamorphism to have occurred at ~1000 Ma. Thus, the petrological signatures and the geochronological data indicate that the effect of 'Rayner orogeny' in the Eastern Ghats Belt can be traced south of Anakapalle at least as far as the Godavari Rift (Rajamundry area) (Fig. 8). This asserts that the continuation of the N–R terrane boundary into the Eastern Ghats Belt should pass between Rajamundry and Kondapalle. It is interesting to note that the Godavari rift passes through this zone and, in the reassembled Indo-Antarctic block, this rift can be linked with the concealed East Enderby rift zone that lies close to the N–R boundary in Enderby Land (Fig. 8). Therefore, the idea of considering the Godavari rift as the N–R boundary in the Eastern Ghats Belt is tempting. Implicit in this assumption is the fact that the Napier complex of East Antarctica and the segment of the south Indian shield lying south of the Godavari rift have shared a similar geological history since Archaean time. In the Napier complex, detailed geochronological evidence indicates that the UHT metamorphism occurred within a narrow time span between 3000 and 2900 Ma [reviewed by Harley & Hensen (1990)]. Notwithstanding the similarity of the UHT metamorphism and the retrograde *P–T* trajectory between the Napier complex and the southern segment of the Eastern Ghats Belt, the timing of such high-grade metamorphism is unknown in the latter segment. This opens up two possibilities: (1) the UHT metamorphic events in these crustal domains are coeval. This means that the Napier complex and the southern segment of the Eastern Ghats are fragments of the same

Archaean block. (2) The UHT metamorphic events in the two domains are temporally unrelated. This means that these domains represent two different crustal segments that were welded together during the ~1000 Ma tectono-thermal event. Recently, Bhaskar Rao *et al.* (1996) have interpreted Sm–Nd whole-rock data on layered complexes at Sittampundi and Bhavani Sagar to document a ~2900 Ma high-grade metamorphic event within the Bhavani–Cauvery shear zone, southern India. In the assembled Indo-Antarctic landmass, this important crustal-scale shear belt juxtaposes against the Napier complex [see Fig. 1 and Bhaskar Rao *et al.* (1996)]. This piece of evidence, although not conclusive, hints at the first option. On the other hand, the western part of the northern sector exposes a zone dominated by basic to enderbitic granulites [the western charnockite zone of Nanda & Pati (1989)] that shows similarities with the igneous association of the southern sector (e.g. at Kondapalle and Ongole). Similarly, a suite of supracrustal granulites occurs in the easternmost parts of the southern sector. In the absence of geochronological data, however, the correlation of the magmatic and the supracrustal rock units across the Godavari rift remains unclear. It also needs to be ascertained through detailed geochronological work whether these supracrustal granulites of the southern sector have been involved in the ~1000 Ma tectono-thermal event. If so, then the Napier complex would represent an isolated nucleus separated by the ~1000 Ma mobile belts. A comprehensive petrological study and, in particular, modern isotope dating of the two segments of the Eastern Ghats Belt is, therefore, needed to allow their crustal evolution to be deciphered and to allow more definite terrane correlations in East Gondwana.

ACKNOWLEDGEMENTS

This work was completed when P.S. and S.D. were in the Mineralogisch–Petrologisches Institut, Bonn, as fellows of the Alexander von Humboldt Stiftung. We also acknowledge the financial assistance from DST, India (to P.S. and S.D.), CSIR, India (to U.K.B.) and the DFG, Germany (to M.R. and J.E.). We thank Subhasis Roychowdhury, Dibyakanti Mukhopadhyay and Sudip Bhattacharya for their assistance during the field work, and Supratim Pal for his help during the preparation of the final version of this paper. We are indebted to Professor Klaus Mezger for stimulating discussion on the possible Indo-Antarctic fit. We are also thankful to him for providing us with his manuscript submitted to *Precambrian Research*. This paper has been greatly benefited from the constructive criticism of Professors J. Sheraton and S. L. Harley. We also thank Professor R. Arculus for his editorial work.

REFERENCES

Aftalion, M., Bowes, D. R., Dash, B. & Dempster, T. J. (1988). Late Proterozoic charnockites in Orissa, India: a U–Pb and Rb–Sr isotopic study. *Journal of Geology* **96,** 663–675.

Annersten, H. & Seifert, F. (1981). Stability of the assemblage orthopyroxene–sillimanite–quartz in the system MgO–FeO–Al_2O_3–SiO_2–H_2O. *Contributions to Mineralogy and Petrology* **77,** 158–165.

Anovitz, L. M. & Essene, E. J. (1987). Compatibility of geobarometers in the system CaO–FeO–Al_2O_3–SiO_2–TiO_2, implications for garnet mixing models. *Journal of Geology* **95,** 633–645.

Ballhaus, C. & Berry, R. T. (1991). Crystallization pressure and cooling history of the Giles layered igneous complex, central Australia. *Journal of Petrology* **32,** 1–28.

Barton, M. D., Staude, J. M, Snow, E. A. & Johnson, A. (1991). Aureole systematics. In: Kerrick, D. M. (ed.) *Contact Metamorphism. Mineralogical Society of America, Reviews in Mineralogy* **26,** 723–846.

Bhaskar Rao, Y. J., Chetty, T. R. K., Janardhan, A. S. & Gopalan, K. (1996). Sm–Nd and Rb–Sr ages and *P–T* history of the Archaean Sittampundi and Bhavani layered meta-anorthosite complexes in Cauvery shear zone, South India: evidence for Neoproterozoic reworking of Archaean crust. *Contributions to Mineralogy and Petrology* **125,** 237–250.

Bhattacharya, A., Krishnakumar, K. R., Raith, M. & Sen, S. K. (1991). An improved set of *a–X* parameters for Fe–Mg–Ca garnets and refinements of the orthopyroxene–garnet–plagioclase–quartz barometer. *Journal of Petrology* **32,** 629–656.

Bohlen, S. R. (1987). Pressure–temperature–time paths and a tectonic model for the evolution of granulites. *Journal of Geology* **95,** 617–632.

Bohlen, S. R., Dolasse, W. A. & Wall, V. J. (1986). Calibration and application of spinel equilibria in the system FeO–Al_2O_3–SiO_2. *Journal of Petrology* **27,** 1143–1156.

Buddington, A. F. & Lindsley, D. H. (1964). Iron–titanium oxide minerals and synthetic equivalents. *Journal of Petrology* **5,** 310–357.

Carrington, D. P. & Harley, S. L. (1995). Partial melting and phase relations in high grade metapelites: an experimental petrogenetic grid in the KFMASH system. *Contributions to Mineralogy and Petrology* **120,** 270–291.

Carrington, D. P. & Watt, G. R. (1995). A geochemical and experimental study of the role of K-feldspar during water-undersaturated melting of pelites. *Chemical Geology* **122,** 59–76.

Chetty, T. R. K. (1995). A correlation of Proterozoic shear zones between Eastern Ghats Belt, India and Enderby Land, east Antarctica, based on LANDSAT imagery. *Memoir, Geological Society of India* **34,** 205–220.

Clarke, G. L. & Powell, R. (1991). Decompressional coronas and symplectites in granulites of the Musgrave complex, central Australia. *Journal of Metamorphic Geology* **9,** 441–450.

Clarke, G. L., Powell, R. & Guiraud, M. (1989). Low pressure granulite facies metapelitic assemblages and corona textures from McRobertson Land, East Antarctica: the importance of Fe_2O_3 and TiO_2 in accounting for spinel-bearing assemblages. *Journal of Metamorphic Geology* **7,** 323–335.

Clemens, J. D. & Vielzeuf, D. (1987). Constraints on melting and magma production in the crust. *Earth and Planetary Science Letters* **86,** 287–306.

Dasgupta, S. & Sengupta, P. (1995). Ultrametamorphism in Precambrian Granulite terrains—evidence from Mg–Al granulites and calc-granulites of the Eastern Ghats, India. *Geological Journal* **30,** 307–318.

Dasgupta, S., Sengupta, P., Mondal, A. & Fukuoka, M. (1993). Mineral chemistry and reaction textures in metabasites from the Eastern Ghats Belt, India. *Mineralogical Magazine* **57,** 113–120.

Dasgupta, S., Sengupta, P., Ehl, J., Raith, M. & Bardhan, S. (1995). Reaction textures in a suite of spinel granulites from the Eastern Ghats Belt, India: evidence for polymetamorphism, a partial petrogenetic grid in the system KFMASH and the roles of ZnO and Fe_2O_3. *Journal of Petrology* **36,** 435–461.

Dasgupta, S., Ehl, J., Raith, M., Sengupta, P. & Sengupta, Pr. (1997). Mid-crustal contact metamorphism around the Chimakurthy mafic–ultramafic complex, Eastern Ghats Belt, India. *Contributions to Mineralogy and Petrology* **129,** 182–197.

Davidson, P. M. & Lindsley, D. H. (1989). Thermodynamic analysis of pyroxene–olivine–quartz equilibria in the system CaO–MgO–FeO–SiO_2. *American Mineralogist* **74,** 18–30.

Ellis, D. J. & Green, D. H. (1979). An experimental study of the effect of Ca upon garnet–clinopyroxene Fe–Mg exchange equilibria. *Contributions to Mineralogy and Petrology* **71,** 13–22.

Ellis, D. J. & Green, D. H. (1985). Garnet-forming reactions in mafic granulites from Enderby Land, Antarctica—implications for geothermometry and geobarometry. *Journal of Petrology* **26,** 633–662.

Federov, L. V., Ravich, M. G. & Hoffman, J. (1982). Geologic comparison of southeastern Peninsular India and Sri Lanka with a part of East Antarctica. In: Craddock, C. (ed.) *Antarctic Geoscience*. Madison, WI: University of Wisconsin Press, pp. 73–78.

Fitzsimons, I. C. W. (1996). Metapelitic migmatites from Brattstrand Bluffs, East Antarctica—metamorphism, melting and exhumation of the mid crust. *Journal of Petrology* **37,** 395–414.

Fitzsimons, I. C. W. & Harley, S. L. (1994). The influence of retrograde cation exchange on granulite *P–T* estimates and a convergence technique for the recovery of peak metamorphic condition. *Journal of Petrology* **35,** 543–576.

Fram, S. M. & Longhi, J. (1992). Phase equilibria of dikes associated with Proterozoic anorthosite complexes. *American Mineralogist* **77,** 605–616.

Frost, B. R. & Frost, C.D. (1987). CO_2, melts and granulite metamorphism. *Nature* **327**, 503–506.

Goscombe, B. (1992). Silica-undersaturated sapphirine, spinel and kornerupine granulite facies rocks, NE Strangways, central Australia. *Journal of Metamorphic Geology* **10,** 181–201.

Grant, J. A. & Frost, B. R. (1990). Contact metamorphism and partial melting of pelitic rocks in the aureole of the Laramie Anorthosite Complex, Morton Pass, Wyoming. *American Journal of Science* **290,** 425–472.

Green, D. H. & Ringwood, A. E. (1967). An experimental investigation of the gabbro to eclogite transformation and its petrological applications. *Geochimica et Cosmochimica Acta* **31,** 767–833.

Grew, E. S. & Manton, W. I. (1986). A new correlation of sapphirine granulites in the Indo-Antarctic metamorphic terrane: Late Proterozoic dates from the Eastern Ghats. *Precambrian Research* **33,** 123–139.

Grew, E. S., Manton, W. I. & James, P. R. (1988). U–Pb data on granulite facies rocks from Fold Island, Kemp Coast, East Antarctica. *Precambrian Research* **42,** 63–75.

Haggerty, S. E. (1976). Oxidation of opaque mineral oxides in basalts. In: Rumble, D. (ed.) *Oxide Minerals. Mineralogical Society of America, Reviews in Mineralogy* **3,** 1–100.

Harley, S. L. (1984). Comparison of the garnet–orthopyroxene geobarometer with recent experimental studies and applications to natural assemblages. *Journal of Petrology* **26,** 819–856.

Harley, S. L. (1989). The origin of granulites: a metamorphic perspective. *Geological Magazine* **126,** 215–247.

Harley, S. L. (1992). Proterozoic granulite terranes. In: Condie, K. C. (ed.) *Proterozoic Crustal Evolution*. Amsterdam: Elsevier, pp. 301–359.

Harley, S. L. & Fitzsimons, I. C. W. (1995). High grade metamorphism and deformation in the Prydz Bay region, East Antarctica: terranes, events and regional correlations. In: Yoshida, M. & Santosh, M. (eds) *India and Antarctica during the Precambrian. Memoir, Geological Society of India* **34,** 73–100.

Harley, S. L. & Hensen, B. J. (1990). Archaean and Proterozoic high grade terranes of East Antarctica (40–80°E): a case study of diversity in granulite facies metamorphism. In: Ashworth, J. R. & Brown, M. (eds) *High Temperature Metamorphism and Crustal Anatexis*. London: Unwin Hyman, pp. 320–370.

Harley, S. L., Hensen, B. J. & Sheraton, J. W. (1990). Two stage decompression in orthopyroxene–sillimanite granulites from Forefinger Point, Enderby Land, Antarctica: implications for the evolution of the Archaean Napier Complex. *Journal of Metamorphic Geology* **8,** 591–613.

Hauck, J. (1981). Crystallography and phase relations of MeO–M_2O_3–TiO_2 systems (Me = Fe, Mg, Ni; M = Al, Cr, Fe). *Journal of Solid State Chemistry* **36,** 52–65.

Hayob, J. L., Essene, E. J., Ruiz, J., Ortega-Gutierrez, F. & Aranda-Gomez, J. J. (1989). Young high-temperature granulites from the base of the crust in central Mexico. *Nature* **342,** 265–268.

Hensen, B. J. (1986). Theoretical phase relations involving cordierite and garnet revisited: the influence of oxygen fugacity on the stability of sapphirine and spinel in the system Mg–Fe–Al–Si–O. *Contributions to Mineralogy and Petrology* **92,** 362–367.

Hensen, B. J. & Harley, S. L. (1990). Graphical analysis of *P–T–X* relations in granulite facies metapelites. In: Ashworth, J. R. & Brown, M. (eds) *High Temperature Metamorphism and Crustal Anatexis*. London: Unwin Hyman, pp. 19–56.

Hensen, B. J. & Motoyoshi, Y. (1988). Sapphirine–quartz–orthopyroxene symplectites after cordierite in granulites from the Napier Complex, Antarctica: evidence for a counter-clockwise *P–T* path? *Terra Cognita* **8,** 263.

Hensen, B. J. & Osanai, Y. (1994). Experimental study of dehydration melting of F-bearing biotite in model pelitic compositions. *Mineralogical Magazine* **58a,** 410–411.

Holland, T. J. B. & Powell, R. (1990). An enlarged and updated internally consistent thermodynamic data set with uncertainties and correlations: the system K_2O–Na_2O–CaO–MgO–FeO–MnO–Fe_2O_3–Al_2O_3–TiO_2–SiO_2–C–H_2–O_2. *Journal of Metamorphic Geology* **8,** 89–124.

Holland, T. J. B., Babu, E. V. S. S. K. & Waters, D. J. (1996). Phase relations of osumilite and dehydration melting in pelitic rocks: a simple thermodynamic model for the KFMASH system. *Contributions to Mineralogy and Petrology* **124,** 383–394.

Irving, A. J. (1974). Geochemical and high pressure experimental studies of garnet pyroxenite and pyroxene granulite xenoliths from the Delegate basaltic pipes, Australia. *Journal of Petrology* **15,** 1–40.

Kamineni, D. C. & Rao, A. T. (1988). Sapphirine granulites from Kakanuru area, Eastern Ghats, India. *American Mineralogist* **73,** 692–700.

Kovach, V. P., Salnikova, E. B., Kotov, A. B., Yakova, S. J. & Rao, A. T. (1997). Pan-African U–Pb zircon age from apatite–magnetite veins of Eastern Ghats granulite belt, India. *Journal of the Geological Society of India* **50,** 421–424.

Koziol, A. M. & Newton, R. C. (1988). Redetermination of the anorthite breakdown reaction and improvement of the plagioclase–garnet–Al_2SiO_5–quartz geobarometer. *American Mineralogist* **73,** 216–223.

Kretz, R. (1983). Symbols for the rock forming minerals. *American Mineralogist* **68,** 277–279.

Kroll, H., Evangelakakis, C. & Voll, G. (1992). Two feldspar geothermometry: a review and revision for slowly cooled rocks. *Contributions to Mineralogy and Petrology* **14,** 510–518.

Lal, R. K., Ackermand, D. & Upadhyay, H. (1987). *P–T–X* relationships deduced from corona textures in sapphirine–spinel–quartz assemblages from Paderu, southern India. *Journal of Petrology* **28,** 1139–1168.

Leelanandam, C. (1990). The anorthosite complexes and Proterozoic mobile belt of Peninsular India: a review. In: Naqvi, S. M. (ed.) *Precambrian Continental Crust and its Economic Resources*. Amsterdam: Elsevier, pp. 409–435.

Leelanandam, C. (1997). The Kondapalle Layered Complex, Andhra Pradesh, India: a synoptic overview. *Gondwana Research* **I**(1), 95–114.

Lee, H. Y. & Ganguly, J. (1988). Equilibrium compositions of coexisting garnet and orthopyroxene: experimental determination in the system FeO–MgO–Al_2O_3–SiO_2 and applications. *Journal of Petrology* **29,** 93–113.

Mezger, K. & Cosca, M. A. (1999). The thermal history of the Eastern Ghats Belt (India), as revealed by U–Pb and ^{40}Ar–^{39}Ar dating of metamorphic and magmatic minerals: implications for the SWEAT correlation. *Precambrian Research* **94,** 251–271.

Mezger, K., Cosca, M. A. & Raith, M. (1996). Thermal history of the Eastern Ghats Belt (India) deduced from U–Pb and Ar–Ar dating of metamorphic minerals. *Journal of Conference Abstracts* **1,** 401.

Moecher, D. P., Essene, E. J. & Anovitz, L. M. (1988). Calculation and application of clinopyroxene–garnet–plagioclase–quartz geobarometers. *Contributions to Mineralogy and Petrology* **92,** 92–106.

Montel, J. M., Weber, C. & Pichavant, M. (1986). Biotite–sillimanite–spinel assemblages in high grade metamorphic rocks: occurrence, chemographic analysis and thermodynamic interest. *Bulletin de Minéralogie* **109,** 555–573.

Mukhopadhyay, A. K. & Bhattacharya, A. (1997). Tectonothermal evolution of the gneiss complex at Salur in the Eastern Ghats granulite belt of India. *Journal of Metamorphic Geology* **15,** 719–734.

Nanda, J. K. & Natarajan, V. (1980). Anorthosites and related rocks of the Kondapalle Hills, Andhra Pradesh. *Records of the Geological Survey of India* **113**(5), 57–67.

Nanda, J. K. & Pati, U. C. (1989). Field relations and petrochemistry of the granulites and associated rocks in the Ganjam–Koraput sector of the Eastern Ghats belt. *Indian Minerals* **43,** 247–264.

Nell, J., Wood, B. J. & March, T. O. (1989). High-temperature cation distribution in Fe_3O_4–$MgAl_2O_4$–$MgFe_2O_4$–$FeAl_2O_4$ spinels from thermopower and conductivity measurements. *American Mineralogist* **74,** 339–351.

Newton, R. C. (1983). Geobarometry in high grade metamorphic rocks. *American Journal of Science* **283A,** 1–28.

Nichols, G. T., Berry, R. F. & Green, D. H. (1992). Internally consistent gahnitic spinel–cordierite–garnet equilibria in the FMASHZn system: geothermobarometry and applications. *Contributions to Mineralogy and Petrology* **111,** 362–377.

Pal, S. & Bose, S. (1997). Mineral reactions and geothermobarometry in a suite of granulite facies rocks from Paderu, Eastern Ghats granulite belt: a reappraisal of the *P–T* trajectory. *Proceedings, Indian Academy of Science* **106,** 77–89.

Paul, D. K., Ray Barman, T. K., McCraughton, M. J., Fletcher, I. R., Potts, P. J., Ramakrishnan, M. & Augustine, P. F. (1990). Archaean–Proterozoic evolution of Indian charnockites. Isotopic and geochemical evidence from granulites of the Eastern Ghats Belt. *Journal of Geology* **98,** 253–263.

Perkins, D. & Chipera, S. J. (1985). Garnet–orthopyroxene–plagioclase–quartz barometry: refinement and application to the English River subprovince and the Minnesota River Valley. *Contributions to Mineralogy and Petrology* **89,** 69–80.

Pouchou, J. L. & Pichoir, F. (1984). A new model for quantitative X-ray microanalysis, Part I: Application to the analysis of homogeneous samples. *La Recherche Aérospatiale* **3,** 167–192.

Powers, R. E. & Bohlen, S. R. (1985). The role of synmetamorphic igneous rocks in the metamorphism and partial melting of metasediments, north-west Adirondacks. *Contributions to Mineralogy and Petrology* **90,** 401–409.

Raith, M., Karmakar, S. & Brown, M. (1997). Ultra-high-temperature metamorphism and multistage decompressional evolution of sapphirine granulites from the Palni Hill ranges, southern India. *Journal of Metamorphic Geology* **15,** 379–399.

Sack, R. O. & Ghiorso, M. S. (1991). An internally consistent model for the thermodynamic properties of Fe–Mg-titano-magnetite–aluminate spinels. *Contributions to Mineralogy and Petrology* **106,** 474–505.

Sen, S. K., Bhattacharya, S. & Acharyya, A. (1995). A multi-stage pressure–temperature record in the Chilka lake granulites: the epitome of the metamorphic evolution of Eastern Ghats, India? *Journal of Metamorphic Geology* **13,** 287–298.

Sengupta, P., Dasgupta, S., Bhattacharya, P. K., Fukuoka, M., Chakraborti, S. & Bhowmick, S. (1990). Petrotectonic imprints in the sapphirine granulites from Anantagiri, Eastern Ghats Mobile Belt, India. *Journal of Petrology* **31,** 971–996.

Sengupta, P., Karmakar, S., Dasgupta, S. & Fukuoka, M. (1991). Petrology of spinel granulites from Araku, Eastern Ghats, India, and a petrotectonic grid for sapphirine-free rocks in the system FMAS. *Journal of Metamorphic Geology* **9,** 451–459.

Shulters, J. C. & Bohlen, S. R. (1989). The stability of hercynite and hercynite–gahnite spinels in corundum or quartz-bearing assemblages. *Journal of Petrology* **33,** 1017–1031.

Srogi, L., Wagner, M. E. & Lutz, T. M. (1993). Dehydration partial melting and disequilibrium in the granulite-facies Wilmington complex, Pennsylvania–Delaware Piedmont. *American Journal of Science* **293,** 405–462.

Subramaniam, A. P. (1959). Charnockites of the type area near Madras—a reinterpretation. *American Journal of Science* **257,** 321–353.

Unrug, R. (1995). Rodinia and Gondwana: a record of supercontinent configuration change. In: Yoshida, M. & Santosh, M. (eds) *India and Antarctica during the Precambrian. Memoir, Geological Society of India* **34,** 1–9.

Vinogradov, A., Tuganiov, A., Zykov, C., Stapnikov, N., Bibikova, E. & Khorre, K. (1964). Geochronology of the Indian Precambrian. *International Geological Congress, 22nd Session, Indian Report* **10,** 553–567.

Waters, D. J. (1991). Hercynite–quartz granulites: phase relations and implications for crustal processes. *European Journal of Mineralogy* **3,** 367–386.

Wells, P. R. A. (1980). Thermal models for the magmatic accretion and subsequent metamorphism of continental crust. *Earth and Planetary Science Letters* **46,** 253–265.

Wickham, S. M. & Oxburgh, E. R. (1985). Continental rifts as a setting for regional metamorphism. *Nature* **318,** 330–333.

Wood, B. J. & Banno, S. (1973). Garnet–orthopyroxene and orthopyroxene–clinopyroxene relationships in simple and complex systems. *Contributions to Mineralogy and Petrology* **42,** 109–124.

Yoshida, M. (1995). Assembly of East Gondwanaland during the Mesoproterozoic and its rejuvenation during the Pan-African period. In: Yoshida, M. & Santosh, M. (eds) *India and Antarctica during the Precambrian. Memoir, Geological Society of India* **34,** 25–46.